Development/Plasticity/Repair

The GTPase Arl8B Plays a Principle Role in the Positioning of Interstitial Axon Branches by Spatially Controlling Autophagosome and Lysosome Location

Gee Adnan,[1] Aine Rubikaite,[1] Moqadisa Khan,[1] Michael Reber,[2] Philip Suetterlin,[1,3] Robert Hindges,[1,4] and Uwe Drescher[1,4]

[1]Centre for Developmental Neurobiology, King's College London, London SE1 1UL, United Kingdom, [2]Krembil Research Institute, Toronto, Ontario M5T 0S8, Canada, [3]Craniofacial Development and Stem Cell Biology, King's College London, Guy's Hospital, London SE1 9RT, United Kingdom, and [4]MRC Centre for Neurodevelopmental Disorders, King's College London, London SE1 1UL, United Kingdom

Interstitial axon branching is an essential step during the establishment of neuronal connectivity. However, the exact mechanisms on how the number and position of branches are determined are still not fully understood. Here, we investigated the role of Arl8B, an adaptor molecule between lysosomes and kinesins. In chick retinal ganglion cells (RGCs), downregulation of Arl8B reduces axon branch density and shifts their location more proximally, while Arl8B overexpression leads to increased density and more distal positions of branches. These alterations correlate with changes in the location and density of lysosomes and autophagosomes along the axon shaft. Diminishing autophagy directly by knock-down of atg7, a key autophagy gene, reduces branch density, while induction of autophagy by rapamycin increases axon branching, indicating that autophagy plays a prominent role in axon branch formation. *In vivo*, local inactivation of autophagy in the retina using a mouse conditional knock-out approach disturbs retino-collicular map formation which is dependent on the formation of interstitial axon branches. These data suggest that Arl8B plays a principal role in the positioning of axon branches by spatially controlling autophagy, thus directly controlling formation of neural connectivity in the brain.

Key words: **autophagy; axon branching; lysosomes; neural circuit development; retinotectal projection; vesicle trafficking**

Significance Statement

The formation of interstitial axonal branches plays a prominent role in numerous places of the developing brain during neural circuit establishment. We show here that the GTPase Arl8B controls density and location of interstitial axon branches, and at the same time controls also density and location of the autophagy machinery. Upregulation or downregulation of autophagy *in vitro* promotes or inhibits axon branching. Local disruption of autophagy *in vivo* disturbs retino-collicular mapping. Our data suggest that Arl8B controls axon branching by controlling locally autophagy. This work is one of the first reports showing a role of autophagy during early neural circuit development and suggests that autophagy in general plays a much more prominent role during brain development than previously anticipated.

Introduction

Axonal branches, which extend interstitially from axon shafts and arborize at specific target locations, are responsible for most, if not all, neural connectivity in the vertebrate CNS (Gallo, 2011; Kalil and Dent, 2014).

The formation of interstitial branches requires cytoskeletal rearrangements at branch points. Here, actin assembly often initiates filopodium formation followed by microtubule (MT) invasion which marks the maturation of the interstitial branches. Various processes have been implicated in controlling these cytoskeletal rearrangements. These include local signaling by membrane-bound receptors (e.g., EphA/ephrinAs; BDNF/TrkB; Yates et al., 2001; Marler et al., 2008), local transport and translation of specific RNAs to sites of emerging branches (Wong et al., 2017; Cioni et al., 2019), and the capture of mitochondria (Courchet et al., 2013; Lewis et al., 2018).

In *Caenorhabditis elegans*, local assembly of an F-actin network initiates synapse formation and axon branching in parallel

Received July 23, 2019; revised July 13, 2020; accepted July 20, 2020.

Author contributions: M.R., P.S., R.H., and U.D. designed research; G.A., A.R., M.K., M.R., P.S., R.H., and U.D. performed research; G.A., A.R., M.K., M.R., P.S., and U.D. analyzed data; U.D. wrote the paper.

This work was supported by the Royal Society Grant IE150445 and the Biotechnology and Biological Sciences Research Council Grant E015522/1 (to U.D.). We would like to thank Jon Clarke, Matthew Dawson and Manolis Fanto for instructive and insightful comments on the manuscript; Alexis Danielle Guerra (University of Irvine, California) and Regina Baranyi (KCL) for technical assistance; and Luke Smith (KCL) for reagents.

The authors declare no competing financial interests.

Correspondence should be addressed to Uwe Drescher at uwe.drescher@kcl.ac.uk.

https://doi.org/10.1523/JNEUROSCI.1759-19.2020

(Chia et al., 2014). Local clustering of synaptic vesicles (SVs) can trigger the development of axonal branches and arborization, as described in the synaptotropic hypothesis (Vaughn, 1989; Alsina et al., 2001; Meyer and Smith, 2006; Ruthazer et al., 2006; Cline and Haas, 2008; Matsumoto et al., 2016; Constance et al., 2018). It is not clear though which factors determine where presynaptic clusters are formed. In *C. elegans*, the small GTPase Arl8 has been shown to determine the position and number of presynaptic sites along axons of DA9 neurons (Klassen et al., 2010; Wu et al., 2013). Arl8 is also involved in the maintenance of presynaptic structures in *Drosophila*, mediating axonal cotransport of active zone (AZ) proteins and SV proteins in lysosome-related vesicles (Vukoja et al., 2018; Goel et al., 2019).

Arl8 belongs to the Ras superfamily of small GTP-binding proteins that switch between a membrane- and GTP-bound active form, and a cytosolic, inactive GDP-bound form (Gillingham and Munro, 2007). While members of the extended families of Arf and Arf-like (Arls) molecules participate in various aspects of membrane organelle traffic, Arl8 is the only G protein localized specifically on lysosomes (Bagshaw et al., 2006; Garg et al., 2011; Korolchuk et al., 2011; Rosa-Ferreira and Munro, 2011; Khatter et al., 2015b).

Lysosomes are a central hub of cellular homeostasis. They degrade and recycle cell-intrinsic structures and extracellular material (Harris and Rubinsztein, 2011; Hurley and Schulman, 2014; Feng et al., 2015), and control metabolic signaling, plasma membrane repair, exocytosis, cell adhesion and migration (Pu et al., 2016). The subcellular location of lysosomes is of crucial importance for their activity (Wong and Cuervo, 2010; Korolchuk et al., 2011; Galluzzi et al., 2014; Hurley and Schulman, 2014; Pu et al., 2016; Bonifacino and Neefjes, 2017; Ferguson, 2018). For example, engulfment of cytoplasmic proteins and organelles by autophagosomes attracts lysosomes and enables their fusion to autolysosomes and the later degradation of engulfed material (Maday et al., 2012; Bento et al., 2013; Maday and Holzbaur, 2014; Filipek et al., 2017; Pu et al., 2017).

Arl8B has been identified as a key regulator of lysosome movement (for review, see Khatter et al., 2015a), functioning as an adaptor molecule linking lysosomes to MT-bound kinesin motor proteins to mediate an MT plus-end directed transport (Hofmann and Munro, 2006; Korolchuk et al., 2011; Pu et al., 2015; Niwa et al., 2016, 2017; Farías et al., 2017).

Arl8B regulates not only the transport of lysosomes into axons (Farías et al., 2017; Rosa-Ferreira et al., 2018) but is also involved in their fusion with autophagosomes and late endosomes by recruiting the homotypic fusion and protein sorting (HOPS) complex (Khatter et al., 2015b; McEwan et al., 2015; Marwaha et al., 2017; Boda et al., 2019).

Here, we show that Arl8B controls the positioning and density of interstitial branching of retinal ganglion cell (RGC) axons, and at the same time controls also positioning and density of lysosomes and autophagosomes. This suggests that Arl8B plays a major role in defining the earliest stages of axon branch formation by locally controlling the dynamics of vesicles involved in autophagy.

Materials and Methods

Cloning of Arl8B expression constructs

Chicken Arl8B cDNA was generated using primers 5′−GCCATGT TGGCGCTGCTCTC−3′ and 3′−ACCTCCAGGACCTCCTGGACCT CCGCTTCTTCTAGACTTTGAATGCTG−3′ from reverse transcribed chick retinal RNA as a template. This cDNA was cloned into expression vectors containing either tdTomato or GFP fluorescent proteins. Here, expression of the fusion proteins (NH_2- Arl8B-tdTomato/GFP-COOH) is under the control of the CMV and β-actin (CAG) promoter. The LAMP-YFP and the fluorescent-LC3 plasmids were purchased from Addgene (plasmid no. 1816) and a gift of Terje Johansen (Tromso, Norway).

Mouse Arl8B cDNA was cloned from mouse brain RNA using RT-RCR into the same vectors with forward primer 5′−GCTTCTCCGGG ATTTTGAGTGTTGAA−3′ and reverse primer 5′−GCTTCTCCGGG ATTTTGAGTGTTGAA−3′. All expression constructs generated by RT-PCR were sequence verified.

Primary chick neuronal cultures

Primary chick retinal cultures were prepared as described in Marler et al. (2008). In brief, nasal retinas were isolated from embryonic day (E)7 or E8 chicken embryos, dissociated to obtain a single-cell suspension and electroporated using an Amaxa Nucleofector (Lonza). Neuronal cultures were plated on poly-L-lysine (Sigma), laminin (Life Technologies)-coated and merosine (Millipore)-coated surfaces and grown for 2–3 d at 37°C in Neurobasal medium (Life Technologies), supplemented with B27 (Life Technologies), L-glutamine (Invitrogen), and forskolin (Sigma) in presence of penicillin/streptomycin (Life Technologies).

Antibody staining

After 2–3 d in culture, retinal neuronal cultures were fixed using 4% paraformaldehyde (PFA), 30% sucrose in PBS, and stained for endogenous expression of Arl8B using a rabbit anti-Arl8B antibody (13049-1-AP from Proteintech), which was raised by immunization with a human ARL8B fusion protein.

In brief, after PFA fixation, cells were three times washed with 1× PBS, 0.1% Triton X-100 (PBST). For antigen retrieval, cells were incubated for 1 h at 60°C in 0.1 M citrate buffer, pH 6.0, and washed four times in PBST, blocked in 5% BSA/10% donkey serum/0.1% Triton X-100 (Blocking buffer-1) for 2 h min at room temperature (RT), incubated with first antibody (anti-Arl8B diluted 1:100; anti-β tubulin 1:500) in Blocking buffer-2 (1% BSA; 5% donkey serum; 0.1% Triton X-100; for specificity control in Blocking buffer-2 only) at 4°C overnight, washed four times in PBST, incubated with anti-rabbit Alexa Fluor 488 antibody (1:1000); anti-mouse Alexa Fluor 647 antibody in Blocking buffer-2 for 2 h at RT, washed four times in PBST, and stored under Mowiol. Analyses were done using a Zeiss confocal LSM800.

LAMP1 was stained using rabbit anti-LAMP1 antibody (Abcam ab24170). Neurons were counterstained with DAPI (Roche) to visualize cell nuclei.

Arl8B knock-down analysis

For Arl8B knock-down experiments, a series of short hairpin RNAs (shRNAs), expressed from the U6 promoter, were analyzed. These plasmids contained in addition a TagRFP expression cassette allowing the subsequent identification of electroporated axons. To select (the most) efficient shRNAs, these constructs were transfected together with an Arl8B-GFP expression plasmid into Chinese hamster ovary (CHO) cells or primary chick retinal neurons. After 2 d in culture, Arl8B expression levels were determined by Western blot analysis using an anti-GFP antibody (Clontech 632496). Anti-GAPDH antibody was used to normalize Arl8B-GFP band intensities. Western blotting results were quantified using ImageJ and Excel software.

The shRNA showing the strongest downregulation [relative to control (scrambled) shRNAs] was used for further functional characterizations. This shRNA targeted the Arl8B mRNA between nucleotides 322 and 344. ShRNAs that do not target any known mRNA ("scrambled shRNA") were used as a control in knock-down experiments.

Atg7 knock-down analysis

For ATG7 knock-down experiments, the RNA of chicken Atg7 was targeted using the miRNA- based shRNA silencing method (Shan et al., 2009). Several shRNA inserts were assembled by PCR using a series of primers including: FOR1 5′−TGCTGTAGGCTGTATGCTGAAGTC CTTGACCAATATGAACGTTTTGGCCACTGACTGAC−3′, REV1 5′− AGTAACAGGCATCATACACTGAAGTCCTTGACATATGAACGTCA

GTCAGTGGCCAAAAC−3′, followed by FOR2 5′−ATTGCATCG ATTGAAGGCTTGCTGTAGGCTGTATGCTG−3′ and REV2 5′−GC AATGAATTCCAGCAATTTGTTCCATGTGAATGCTAGTAACAGGC ATCATACACTG−3′. The resulting 154-nucleotide fragment was cleaved at ClaI and EcoRI restriction sites and cloned into an eGFP vector, under the control of the CAG promoter (Furukawa et al., 2011). The silencing efficiency was assessed by transfecting various constructs into CHO cells together with an Atg7-Flag-expressing vector. After 3 d in culture, Atg7 expression levels were analyzed by Western blotting using an anti-FLAG antibody (Sigma F1804). As a control, a shRNA plasmid containing sequences that do not target any known mRNA (scrambled shRNA) was used. The shRNA with the strongest knock-down efficiency (sequence shown above) was used for additional experiments.

Chicken Atg7 was amplified from reverse transcribed chick retinal RNA as a template using primers 5′−AAGCTTCAATCATGGCA GCAGTCAGTAATG−3′ and 5′−CTCGAGGACTGTTTCATCATC ACTCATGTCC−3′, 205 cleaved at HindIII and XhoI restriction sites and cloned into the pCMV-3 Tag-3 vector (Agilent).

Experimental design and statistical analyses

The experimental design and statistical analyses are described in detail for every single figure and experiment.

Axon branching assay

To analyze the consequences of upregulation or knock-down of Arl8B, or of Atg7, on axon branching, E7 or E8 single-cell retinal cultures were electroporated with either an Arl8B-GFP expression plasmid, Arl8B (or Atg7) shRNA plasmids, GFP-RFP-LC3 (Jain et al., 2010) or control constructs. Axon branching was analyzed after 3 d in culture.

Generally, for functional knock-down/overexpression experiments, 5–10 μg of DNA was electroporated per single-cell retinal prep, for experiments to visualize particular structures (lysosomes, LC3-II puncta, etc.) including colocalization experiments, only 0.5 μg of DNA per single-cell retinal prep was electroporated.

A total of 5 ng/ml BDNF was added 24 h after plating (Marler et al., 2008). After 3 d *in vitro*, retinal cultures were fixed and imaged by fluorescent microscopy, and axon length and branch number were analyzed using MetaMorph, ImageJ (using the NeuronJ plug-in), Microsoft Excel, and GraphPad Prism software. RGCs were identified based on their neurite morphology and by immunocytochemical staining using RGC-specific antibodies as described previously (Marler et al., 2008).

Only branches longer than 5 μm were considered (Marler et al., 2008; Matsumoto et al., 2016). Branch density was determined as the number of axon branches per unit of axon length. Branch density is given as mean percentage values (normalized against the appropriate control neurons) ± SEM.

All analyses were done blind to the condition. Statistical significance between the conditions was tested using Student's *t* test.

Analysis of particle distribution

RGC axons expressing fusion proteins (GFP, RFP, tdTomato, mCherry) were observed using a confocal Zeiss LSM800 with a 63× objective lens. Tiles were used to capture entire RGCs and stitched using the Carl Zeiss Microscopy software Zen 2.3 (blue edition). Z-stacks captured axonal puncta in their focal plane and were collapsed using the ImageJ tool "Z Project."

ImageJ tools were used to analyze the proximo-distal distribution of lysosomes, autophagosomes, or SV clusters along RGC axons in control, Arl8B KD, Atg7 KD and other approaches (bafilomycin, rapamycin). The segmented line tool was used to trace the axon of each RGC, and the profile of pixel intensities was plotted. A background value, defined as the minimum signal value, was subtracted uniformly from each axon. The sum of pixel intensities of the proximal, middle, and distal one-third compartments was individually calculated as a percentage of the sum of pixel intensities across the axon. The mean of each one-third compartment was calculated per condition. Statistical significance between conditions was tested using Student's *t* test.

Quantification of puncta in axons, colocalization analysis (using coloc2)

The Fiji plugin 'straighten' is used to straighten RGC axons to exclude extracellular noise or irrelevant somatic signals. The amount of colocalization of two fluorescent-labeled proteins in the axon is automatically quantified using the ImageJ plugin 'Coloc 2' (Cioni et al., 2018; Ordonez et al., 2018; Bonanomi et al., 2019). This performs pixel intensity analysis of correlation between the two channels in the straightened axon using Pearson's linear correlation analysis, which gives a correlation coefficient value *r*. As a control for random overlap, Coloc2 shuffles pixel groups of one channel and repeats the correlation analysis against the second channel, giving a second *r* value. Coloc2 also uses the Costes method to test for statistical significance between the *r* values ($p > 0.95$ signify a statistical significance). The mean *r* value for each condition is calculated using Fisher z-transformation.

Quantification of puncta in axons, distribution of low-density puncta

For puncta that naturally occur in very low densities in the axon (such as LC3), a different method was used to quantify their distribution and density with greater accuracy. A series of ImageJ tools were used to quantify puncta density and distribution in the proximo-distal axis of individual axons. All axons were initially traced and straightened using the ImageJ tools "Segmented Line" and "Straighten," respectively. Puncta along each axon were identified using similar thresholding methods to the established Otsu method (Otsu, 1979; Matsumoto et al., 2016), namely "intermodes," which is a histogram-derived thresholding method that operates iterative smoothing until two local maxima remain. This method best identified individual puncta in proximity with each other. The plugin "Particle Analyzer" was used to quantify particles above threshold. Particles were only identified as puncta if they were larger than two pixels (~0.1 μm).

Particle analyzer also allows the proximo-distal coordinates of puncta in a straightened axon to be measured. Each axon was then divided into three equal segments (proximal, middle, and distal thirds) and the coordinates of each punctum was used to quantify the number of puncta in each axon segments. The mean proportion of puncta in each axon segment was then calculated as a percentage for each condition. To calculate relative puncta density, the total number of puncta was divided by the axon length to give puncta density. Puncta densities were normalized to the mean puncta density in controls to give relative puncta density for each axon.

Quantification of density of DiI-labeled termination zones (TZs)

Whole superior colliculi (SC) of *pax6-α:cre; atg7$^{fl/fl}$* mice and *atg7$^{fl/fl}$* mice; cre^{-} mice were carefully dissected out and immediately imaged using a Zeiss Axioscope fluorescence microscope with a 568 nm excitation laser. A 5× objective was used to capture entire SC and any DiI-labeled TZs.

Images were processed and TZs analyzed using ImageJ tools as follows. SCs in all images were outlined as region of interest (ROI) excluding all other signals. TZs were identified using the tool thresholding method "Triangle," a geometric method which assumes a maximum peak in the histogram and best identifies weak TZ signals in the SC. Any background noise was identified using the remaining area of the SC which does not contain a TZ. The density of TZs was finally calculated as the raw integral values (R) minus background noise (B) divided by the area of the TZ (A), which previously was determined by thresholding (TZ density = (R – B)/A)).

The mean TZ density was calculated for each condition and significant difference was determined using an independent-samples *t* test.

Results

Arl8B colocalizes with lysosomes in the axonal compartment

Interstitial axon branching is a critical step during map development in the retino-tectal projection (Yates et al., 2001; Hindges et al., 2002; Marler et al., 2014). Here, RGC axons initially grow into the tectum in a non-topographic manner and "overshoot" their future TZs substantially. Topographically specific interstitial branching subsequently leads to the formation of TZs, and the development of a topographic map. Overshoot axon segments

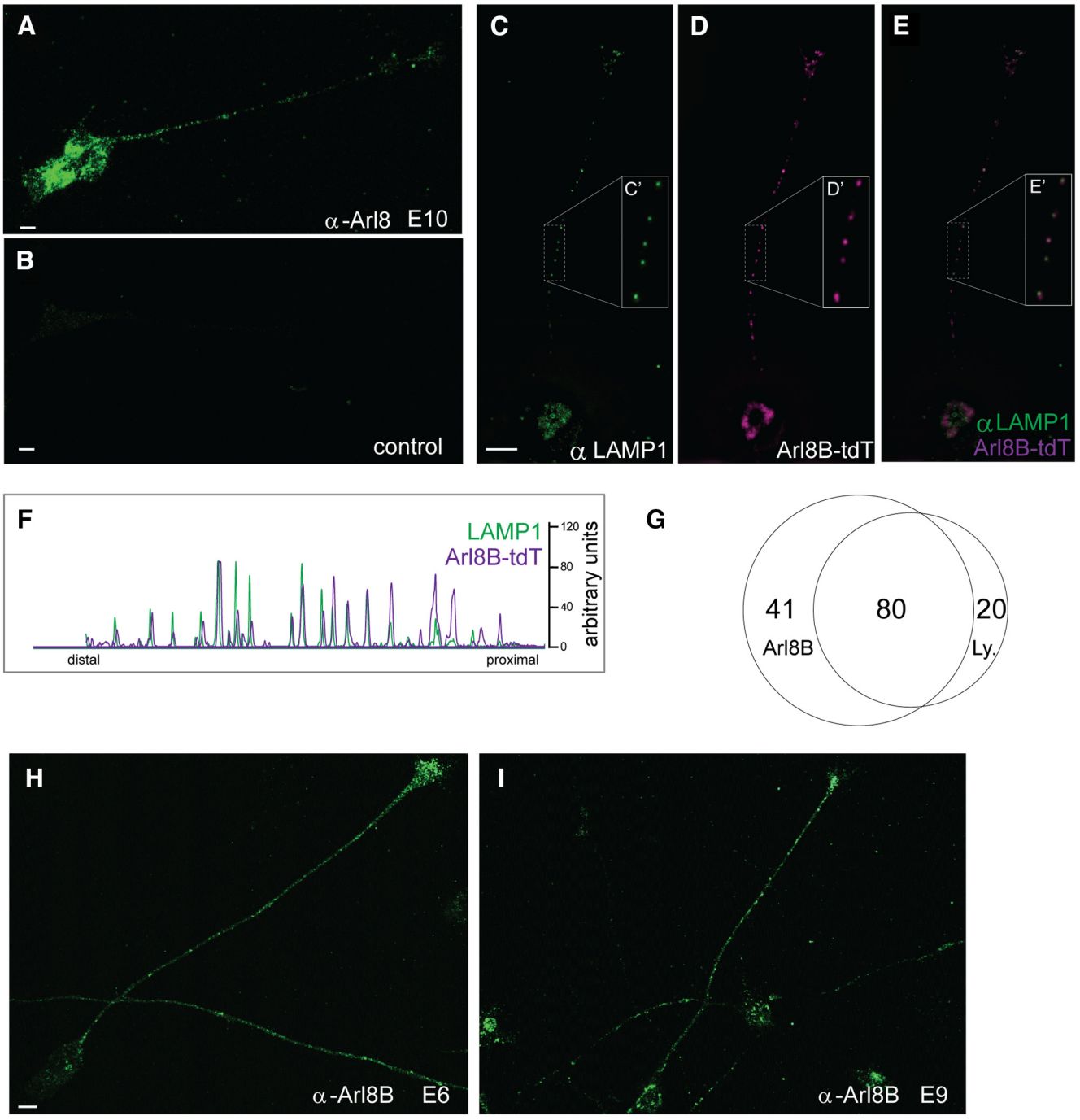

Figure 1. Arl8B is expressed on RGC axons and colocalizes here with LAMP1-positive lysosomes. ***A***, Neuronal cultures derived from E8 chicken retinae were incubated for 2 d and stained with an antibody against Arl8B. Analysis of RGCs shows a punctate staining along the axon. ***B***, Control staining (omitting first antibody) of an RGC axon. Representative examples are shown. Conditions for image acquisition and data processing were identical for ***A***, ***B***. Scale bar: 5 μm. ***C–E***, Colocalization of LAMP1-positive lysosomes (***C***) with Arl8B-tdT (***D***). Single cells from an E8 dissociated retina preparation were electroporated with an Arl8B-tdTomato (Arl8B-tdT) expression construct and incubated for 3 d in culture. Lysosomes were identified by staining with an anti-LAMP1 antibody. Insets (***C'–E'***) show higher magnifications of boxed areas to highlight colocalizations. These analyses were done by super resolution SIM. Scale bar: 10 μm. ***F***, Profile plots of ***C***, ***D***, in which peaks represent the position of puncta along the axon. ***G***, Venn diagram indicating the percentage of colocalization between Arl8-tdT and LAMP1-positive puncta, with 80% LAMP1 puncta positive for Arl8B and 59% Arl8B puncta positive for LAMP1. ***H***, ***I***, Endogenous expression pattern of Arl8B at developmental time points E6 and E9. Scale bar: 5 μm.

are later removed. Members of the EphA/ephrinA family in concert with neurotrophic factors, such as BDNF and NT3, play prominent roles in this branching process (for review, see Suetterlin et al., 2012; Cang and Feldheim, 2013; Weth et al., 2014).

To characterize possible roles of Arl8B in this process, the first step was to determine its subcellular localization along RGC axons. We stained retinal cultures from E8 chicks after 2 d in culture with an Arl8B-specific antibody (see Materials and Methods). This time point corresponds to the major phase of retino-tectal map development between E10 and E14 during which RGC axons form TZs in the tectum through intense interstitial axon branching and subsequent arborization. Our data show a punctate expression pattern throughout the RGC axonal compartment (Fig. 1*A*,*B*).

As Arl8B is bound specifically to lysosomal and late endosomal membranes in vertebrate neuronal and non-neuronal cells

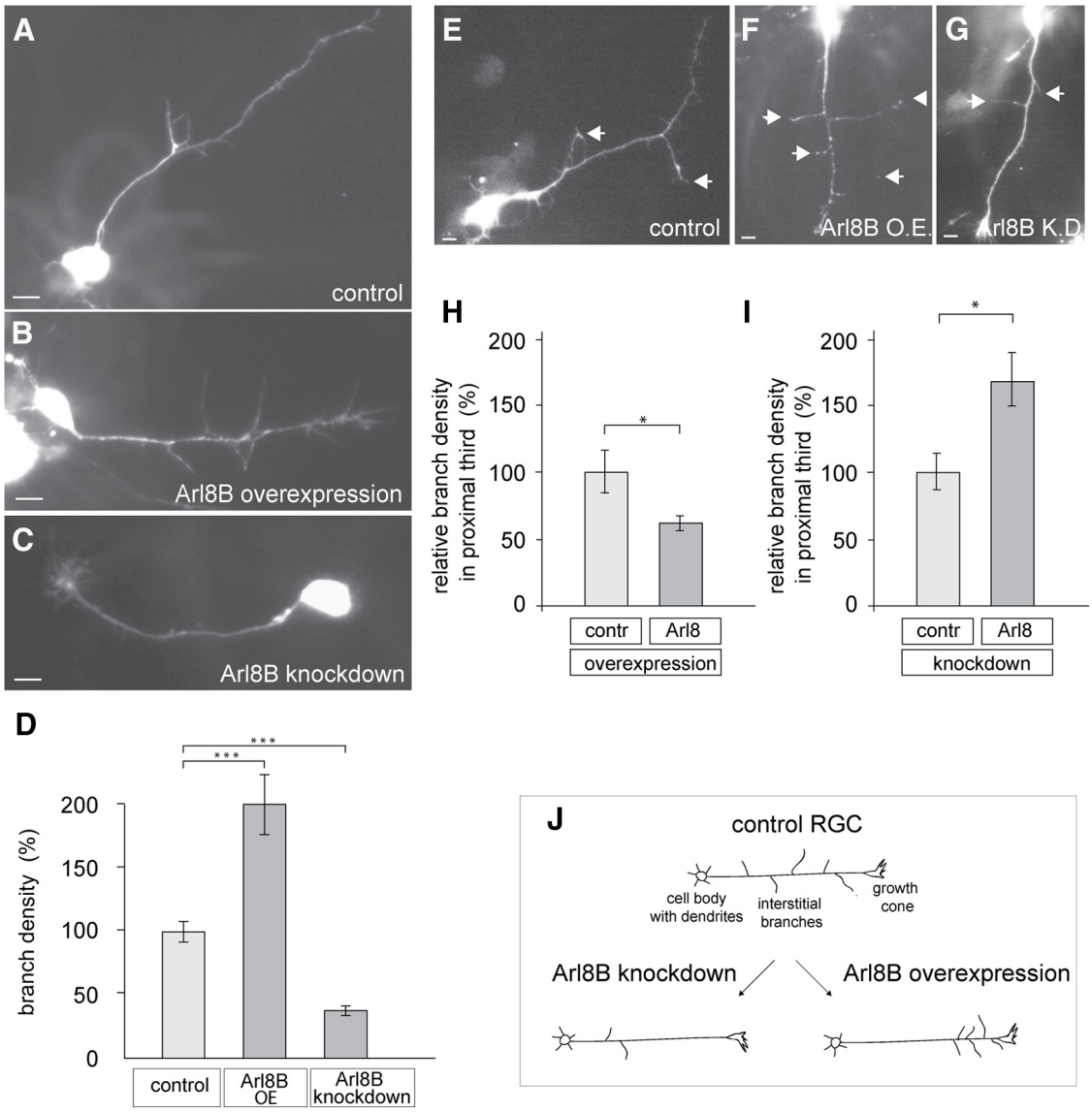

Figure 2. Arl8B controls RGC axon branch density and position. E8 chick single retinal cells were electroporated with expression constructs to either knock-down or to overexpress Arl8B. After 3 d in culture, neurons were fixed, and RGC axon length and branch number determined. Branch density is given as the number of axon branches per unit axon length. The values were normalized against cultures expressing corresponding control constructs. Axon length and branch number were analyzed using MetaMorph and NeuronJ. For each experimental condition, three independent experiments were performed with $n > 15$ axons for each experiment. ***A–D***, After knock-down or overexpression of Arl8B, the density of RGC axon branches was determined. ***A–C***, Representative images of RGC axons from (***A***) control, (***B***) Arl8B overexpression, and (***C***) Arl8B shRNA knock-down. ***D***, Quantification of branch counts in the different conditions. Arl8B overexpression increases the number of axon branches by a factor of ~2 (to 201.1 ± 23.7%; control 100%), while Arl8B knock-down decreased axon branching by about two-thirds to 37.6 ± 3.8%. The characterization of Arl8B shRNA including rescue experiments are shown in Figure 3. Scale bar in ***A–C***: 5 µm. ***E–I***, Determination of the proximo-distal location of RGC axon branches after knock-down or overexpression of Arl8B. ***E–G***, Representative images of RGC axons from control cultures (***E***), Arl8B overexpression (***F***), and Arl8B shRNA knock-down (***G***). ***H***, Arl8B overexpression decreased axon branching to 59.8 ± 5.4% in the proximal third, while (***I***) Arl8B shRNA knock-down increased the fraction of axon branches in the proximal third to 169.4 ± 9.4% (control = 100 ± 9%). Statistical analysis was performed using Student's *t* test. Error bars denote SEM, and significance is indicated as ***$p < 0.001$ and *$p < 0.05$. Scale bar in ***E–G***: 5 µm. ***J***, Schematic summary of the results from overexpression and knock-down of Arl8B on RGC branch location and number.

(see Introduction), we investigated whether this is also true for RGC axons. We expressed an Arl8B-tdTomato fusion protein in E8 single-cell retinal preparations and stained these cultures 3 d later for LAMP1, a specific marker for lysosomes. RGCs were identified based on their neurite morphology and by immunocytochemical staining using RGC-specific antibodies (as previously; Marler et al., 2008). Super-resolution structured illumination microscopy (SIM) showed an extensive colocalization of fluorescently labeled Arl8B with LAMP1 puncta (Fig. 1*C–G*) confirming that in RGC axons Arl8B associates with lysosomes. Approximately 80% of the LAMP1 puncta were positive for Arl8B, while a small fraction of Arl8B-positive puncta was negative for LAMP1 (Fig. 1*F*,*G*). These findings are consistent with recent data from mouse hippocampal neurons (Farías et al., 2017; Vukoja et al., 2018).

A further developmental analysis showed that Arl8B protein, identified by specific antibodies, is localized in axons not only at the time of RGC branching within the tectum (Fig. 1*A*,*I*), but already at E6, a time when RGC axons have just reached this area (Fig. 1*H*), indicating a role of Arl8B beyond axon branching.

Arl8B controls the density of axon branches

To test for a role of Arl8B in controlling interstitial axon branching, we employed both an overexpression and a knock-down approach using shRNAs (Fig. 2).

In the gain of function approach, we analyzed the effects of Arl8B overexpression on axon morphology. We used here an Arl8B-GFP fusion protein which has been shown previously to be functionally intact (Korolchuk et al., 2011). Overexpression of Arl8B-GFP in cultured chick RGCs resulted in a ~2-fold increase in axon branch density [201.1 ± 23.7% (mean ± SEM)] compared with cultures transfected with control plasmid (Fig. 2*A*,*B*,*D*).

For the complementary knock-down approach, primary cultures from E8 chick retina were electroporated with either Arl8B shRNA plasmids (described in Fig. 3) or control shRNA constructs and analyzed by fluorescent microscopy after 3 d in culture. Knock-down of Arl8B resulted in a decrease in interstitial axon branch density (number of axonal branches per unit of axon length) to 37.6 ± 3.8% (mean ± SEM) of branch density in control transfected cultures (= 100%; Fig. 2*A*,*C*,*D*). Arl8B knock-down had no significant effect on axon length (96.34 µm for Arl8B shRNA vs 93.17 µm for control shRNA).

Taken together, these results show that the expression level of Arl8B controls axon branch density in cultured RGCs.

Arl8B expression level affects the location of axon branches

A crucial aspect for the development of the topographically specific formation of TZs during retino-tectal map development is where along the axon branches are formed. We therefore analyzed next whether changing Arl8B expression levels affect also the proximo-distal positioning of branches along RGC axons (Fig. 2*E–I*). We found that overexpression of Arl8B decreased the fraction of branches in the proximal third of axons (Fig. 2*F*, *H*), while a knock-down of Arl8B increases the fraction of branches formed in this area, compared with controls (Fig. 2*G*,*I*). Thus, after Arl8B knock-down, the fraction of branches in the proximal third rose to 169.4 ± 9.4% (mean ± SEM) compared with controls (100%), while upregulation reduced the fraction of branches to 59.8 ± 5.4% (mean ± SEM) of controls (Fig. 2*H*,*I*).

Our results therefore show that Arl8B controls the density and position of RGC axon branches, as schematized in Figure 2*J*.

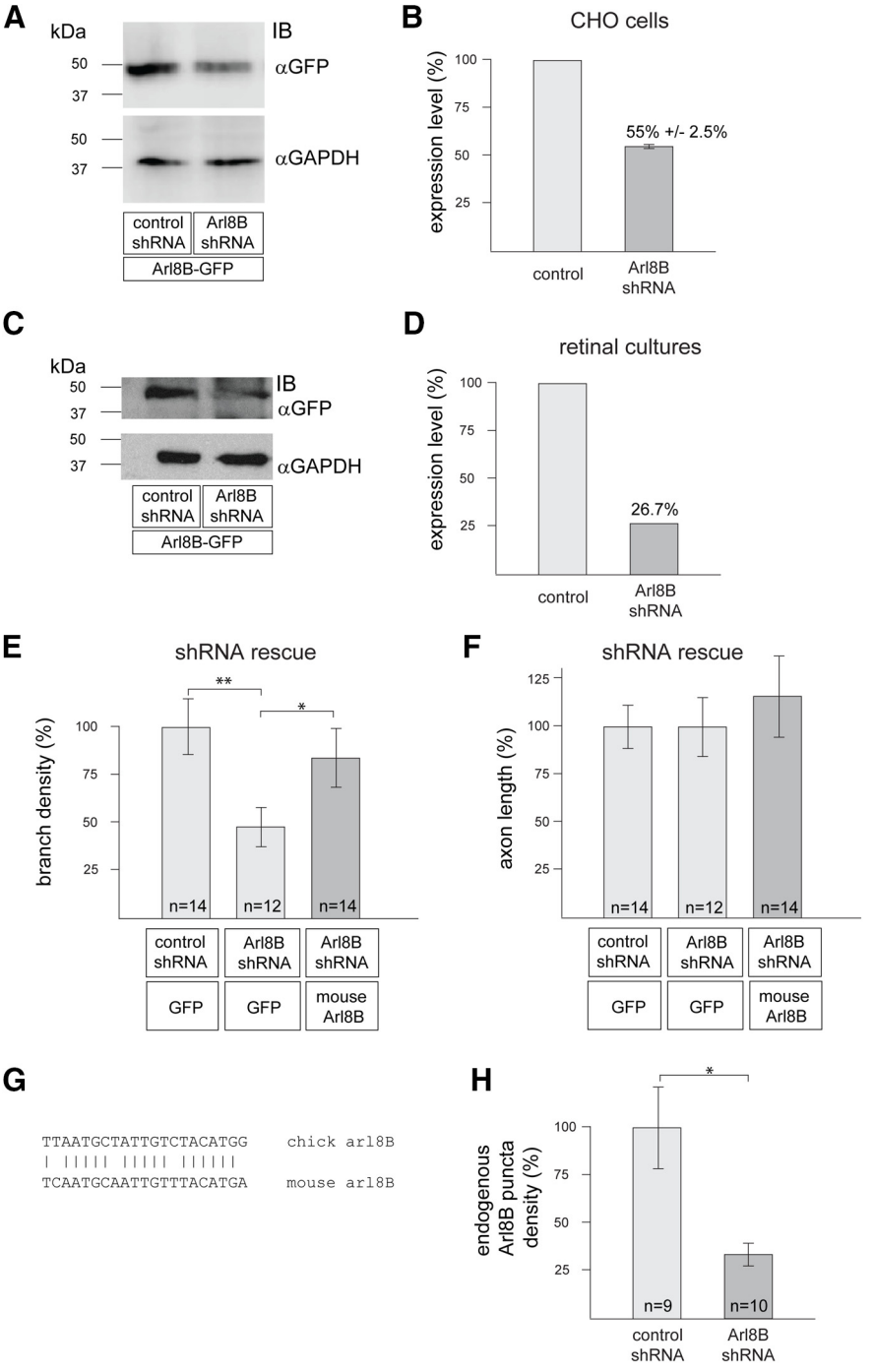

Figure 3. Characterization of shRNAs for chick Arl8B knock-down and rescue experiments. ***A–D***, Arl8-GFP together with either an shRNA specific for Arl8B or a control (scrambled) shRNA were co- electroporated into CHO cells (***A***, ***B***) or E8 retinal cultures (***C***, ***D***). Two days later, cell lysates were investigated in a Western blot analysis using an anti-GFP antibody and for a loading control, an anti-GAPDH antibody (***A***, ***C***). The corresponding quantifications are shown in ***B***, ***D***. Data shown are the result of three (***A***, ***B***) or two (***C***, ***D***) independent experiments. IB: immunoblot. ***E–G***, To demonstrate the specificity of the chick arl8B shRNA, rescue experiments were performed using mouse Arl8B expression constructs. The downregulation of branching density by the shRNA specific for chick Arl8B is fully rescued by overexpression of mouse Arl8B (***E***). Axon length is not affected in these experiments (***F***). A sequence comparison shows four nucleotide differences in the relevant mouse sequence compared with the chick shRNA target sequence (***G***). ***H***, The density of endogenous Arl8B puncta in chick RGC axons is significantly downregulated after Arl8B shRNA transfection. *N* numbers shown within the bars (***E***, ***F***, ***H***) indicate the number of axons analyzed. Error bars represent SEM. The statistical significance is given with $*p < 0.05$ and $**p < 0.01$ using Student's *t* test.

Characterization of Arl8B shRNAs

To confirm their function in knocking down Arl8B, the shRNAs used were transfected together with an Arl8B-GFP expression plasmid into CHO cells or primary chick retinal neurons. After

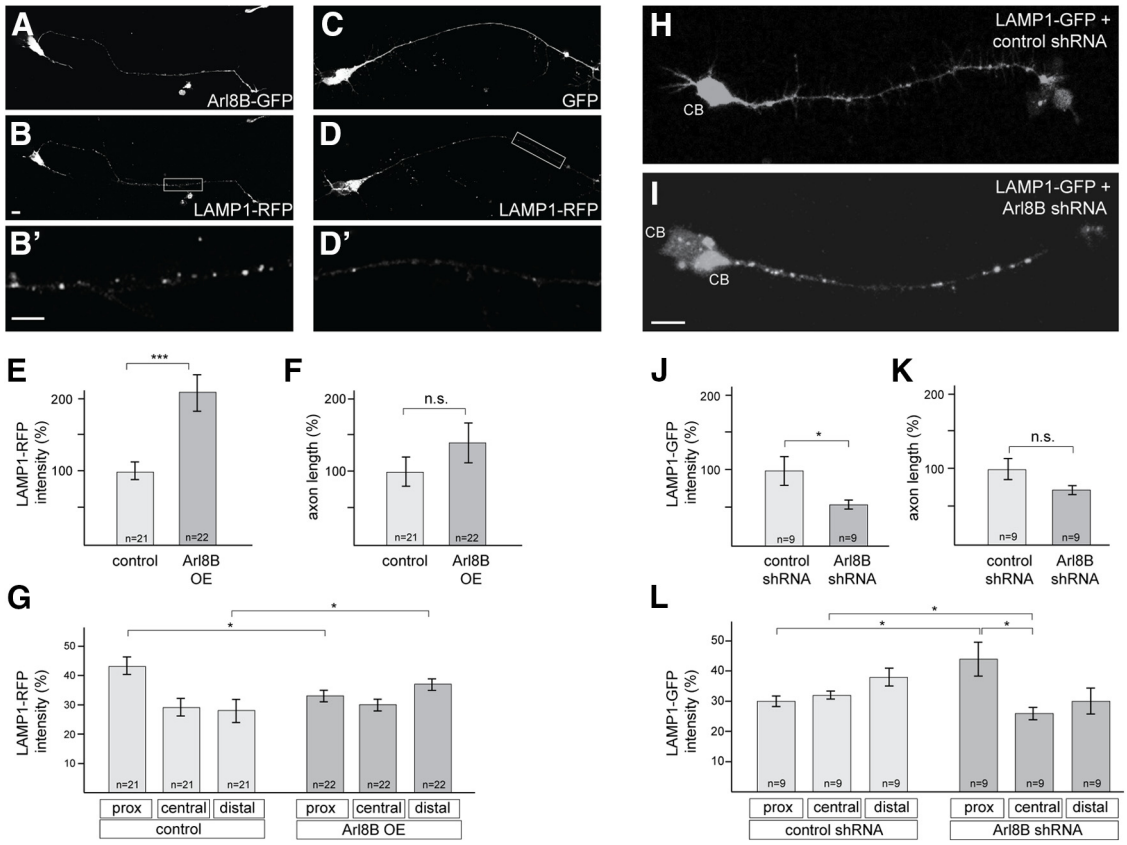

Figure 4. Modulation of Arl8B expression affects density and position of lysosomes in RGC axons. ***A–D***, Retinal cultures were transfected with expression plasmids for Arl8B-GFP (***A***, ***B***, ***B′***) or GFP (***C***, ***D***, ***D′***) and small amounts of LAMP1-RFP (***A–D***) to visualize lysosome distributions. After 3 d in culture, neurones were analyzed for LAMP1-RFP fluorescence intensity and distribution (***E–G***). The sum of three independent experiments is shown. ***B′***, ***D′***, Higher magnifications of axonal segments from ***B***, ***D***, respectively, to illustrate the increase in lysosome density in the distal axon after Arl8B-GFP overexpression. Overexpression of Arl8B-GFP results in a significant increase in the intensity of LAMP1-RFP (***E***). Axon length is not affected (***F***). Lysosome-RFP intensity is decreased in the proximal third of axons, while it is increased in the distal third (***G***). ***H–L***, Retinal cultures were transfected with control shRNA (***H***) or Arl8B shRNA (***I***), together with small amounts of LAMP1-GFP (***H***, ***I***) to visualize lysosome distributions. Cultures were fixed 3 d later and analyzed for LAMP-1-GFP fluorescence distribution along the axons. A quantification of the LAMP1-GFP distribution is given in ***J–L***. Arl8B knock-down results in a significant reduction in the overall intensity of LAMP1-GFP fluorescence (***J***), and a fluorescence shift to the proximal third of axons (***L***). Axon length is not affected (***K***). The quantification method used is described in Materials and Methods. Statistical analysis was performed using Student's *t* test. Error bars denote SEM and significance is indicated as $*p < 0.05$ and $***p < 0.001$; n.s., not significant. The number of axons analyzed (*n*) is given within the columns. Scale bars: 20 μm (***A–D***) and 10 μm (***H***, ***I***). CB: cell body.

2 d in culture, Arl8B-GFP expression levels relative to control (scrambled) shRNA transfected cells were significantly downregulated (Fig. 3*A–D*).

We used branch density as a parameter to further investigate possible off-target effects of the Arl8B shRNA, i.e., its specificity in knocking down Arl8B (Fig. 3*E–G*). For this, we analyzed whether the reduced branch density mediated by the shRNA for chick Arl8B mRNA could be rescued by overexpression of mouse Arl8B protein. A sequence alignment showed a difference in four out of 20 nucleotides between the shRNA target region in the chick sequence, and the corresponding region in the mouse Arl8B sequence (Fig. 3*G*), making it unlikely that the chick shRNA binds to mouse Arl8B mRNA. We found that overexpression of mouse Arl8B rescues the shRNA-mediated down regulation of branching (Fig. 3*E*). We conclude from this that the effect of the chick shRNA is specific for Arl8B and unlikely because of an off-target effect. As before, axon length was not affected by these manipulations (Fig. 3*F*).

Further proof for the specificity of the Arl8B shRNA was obtained by staining axons for endogenous Arl8B protein (see Materials and Methods) after shRNA transfection. We found a strong and statistically significant reduction in Arl8B-positive puncta density for Arl8B shRNA-expressing axons to about a third of the density in axons expressing the control shRNA (Fig. 3*H*).

Arl8B controls the density and location of lysosomes in RGC axons

Arl8B is located on lysosomes (Fig. 1), where it promotes their anterograde transport as an adaptor molecule to kinesin motor proteins (Garg et al., 2011; Rosa-Ferreira and Munro, 2011; Tuli et al., 2013; Pu et al., 2015; Farías et al., 2017; Marwaha et al., 2017), in particular by relieving the autoinhibition of kinesins (Niwa et al., 2016).

We therefore investigated whether the observed proximo-distal shift in relative axon branch position in response to altering Arl8B levels can be correlated with a similar shift in lysosome position (Fig. 4). Retinal cultures were transfected with expression vectors for Arl8B-GFP or control protein (GFP), together with small amounts of a LAMP1-RFP expression vector, to specifically label lysosomes. Three days later, the density of LAMP1-positive puncta and their relative position along RGC axons were analyzed (Fig. 4*A–G*).

Our data show that Arl8B overexpression results in a ~2-fold overall increase in lysosome intensity compared with controls (Fig. 4*E*). We found a particular increase in LAMP1-RFP

fluorescence in the distal axonal compartment, as well as a reduction in fluorescence in the proximal compartment (Fig. 4*G*). Overexpression of Arl8B did not affect axon length (Fig. 4*F*).

In complementary experiments (Fig. 4*H–L*), we found that Arl8B knock-down reduces the overall LAMP1-GFP fluorescence in RGC axons (Fig. 4*J*), while axon length was not affected (Fig. 4*K*). Intriguingly, Arl8B knock-down increases the LAMP1-RFP fluorescence in the proximal part of axons (Fig. 4*L*).

In sum, underscoring its function as an adaptor molecule linking lysosomes and kinesins, we show here that overexpression of Arl8B results in an overall increase in lysosome density and their accumulation in the distal part of RGC axons, while Arl8B knock-down leads to a decrease in the density of lysosomes and their accumulation in the proximal parts of axons.

Thus, our data unravel a striking correlation between lysosome positioning and density, on the one hand, and axon branch positioning and density, on the other hand.

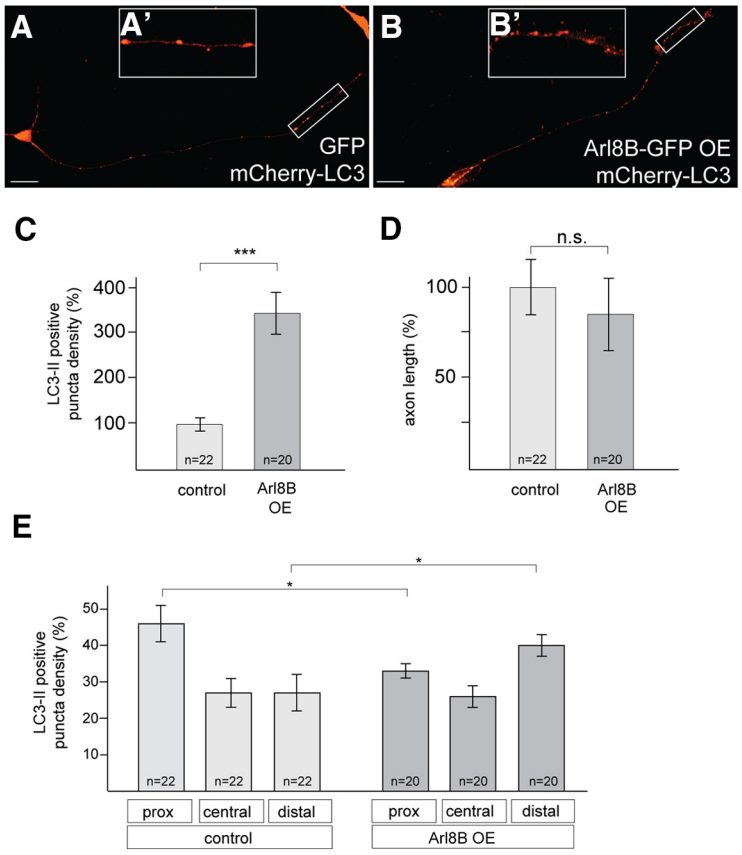

Figure 5. Arl8B controls autophagosome density and position. Single-cell retinal cultures were transfected with expression constructs for either GFP (***A***, control) or Arl8B-GFP (***B***), together with small amounts of mCherry-LC3, and analyzed 3 d later for density and distribution of LC3-II puncta. Inserts (***A′***, ***B′***) represent higher magnifications of the distal part of the axons boxed in ***A***, ***B***, respectively. Overexpression of Arl8B leads to a ~3-fold increase in the density of puncta (***C***), while axon length is unaffected (***D***). Arl8B overexpression leads to a higher density of puncta in the distal third of axons, and a lower density in the proximal part compared with control (***E***). Data summarize the results of two independently conducted experiments. The total number of axons analyzed (*n*) is given within the bars. ***C–E***, Error bars denote SEM. Statistical analyses were done using Student's *t* test; ***$p < 0.001$ and *$p < 0.05$; n.s., not significant. Scale bar in ***A***, ***B***: 10 μm.

Arl8B controls autophagosome density and location

Towards unravelling the mechanisms by which Arl8B-mediated positioning of lysosomes might play a role in positioning interstitial axon branches, we analyzed whether changing the expression level of Arl8B also affects the density or distribution of other components of the autophagy pathway (Fig. 5). For this, we expressed an mCherry-tagged version of LC3, a central protein for autophagosome biogenesis, in retinal neurons enabling us to visualize the formation of autophagosomes, a process that is considered a hallmark of induction of autophagy (Klionsky et al., 2012). The mCherry-LC3 protein normally shows a predominantly cytoplasmic and diffuse staining pattern (LC3-I); however, it is (cleaved and) lipidated during autophagy induction and incorporated into forming autophagosomes (LC3-II) resulting in a punctate (fluorescence) pattern (Klionsky et al., 2012). Thus, the density of puncta of LC3-II can be taken as a read-out for the level of autophagy (Klionsky et al., 2012).

We found that expression of only mCherry-LC3 in RGC axons, that is, at baseline levels of Arl8B, leads to a low density of fluorescent puncta (Fig. 5*A*,*C*), indicating that RGC axons normally contain only a small number of (steady-state) autophagosomes. However, after overexpression of Arl8B, we observed a dramatic, ~3-fold increase in the number of fluorescent mCherry-LC3 puncta (Fig. 5*B*,*C*). This increase was particularly manifest in the distal part of RGC axons, while the density of puncta in the proximal part was reduced compared with controls (Fig. 5*E*). These findings are in good agreement with other reports which showed that overexpression of Arl8B in fibroblast cells leads to an increase in LC3-II levels, i.e., an increase in autophagy (Korolchuk et al., 2011).

Thus, these data show that Arl8B expression levels affect not only the spatial distribution of lysosomes but also the spatial distribution of autophagosomes, such that areas of higher autophagosome density are areas of higher axon branch density. This ultimately suggests that local activation of autophagy is involved in branch formation.

Baseline levels of autophagy are necessary for retinal axon branching

Based on this intriguing correlation between Arl8B-induced axon branching and autophagosome/lysosome distribution, we next asked whether abolishing or increasing autophagy directly would also affect retinal axon branch density.

To study the effects of abolishing autophagy, we knocked down Atg7, a protein whose function is essential for the initiation of autophagosome formation, and which is a validated target to disrupt autophagy (Komatsu et al., 2006, 2007). Using an miR-like shRNA approach (Shan et al., 2009), we identified shRNAs which efficiently knocked down expression of the Atg7 protein (Fig. 6*A*,*B*). To verify that this Atg7 shRNA indeed affects autophagy, we cotransfected Atg7 shRNA and mCherry-LC3 and found a significant reduction in LC3-II puncta density compared with control shRNA transfected neurons (Fig. 6*C*). These results are comparable to an analysis of brain tissue from

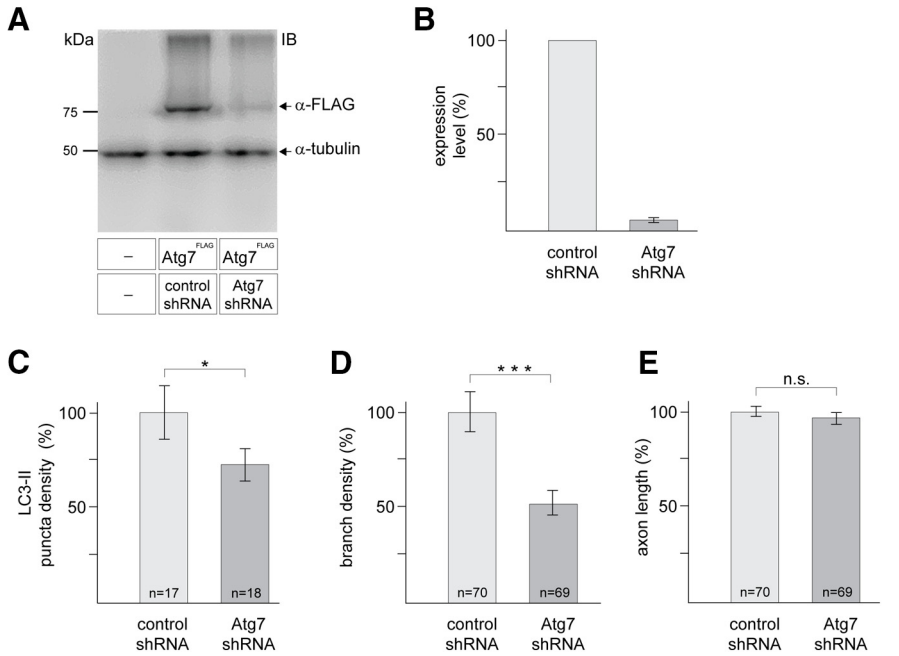

Figure 6. Autophagy controls axon branching. Increasing or decreasing autophagy results in an increase or decrease in RGC axon branch density, respectively. ***A***, ***B***, Characterization of shRNAs for ATG7. ***A***, Plasmids for expression of $Atg7^{Flag}$, and either Atg7 shRNA or a control (scrambled) shRNA plasmids were cotransfected into CHO cells. Three days later, the lysates were investigated in a Western blot analysis using an anti-FLAG antibody and for a loading control, an anti-α-tubulin antibody. ***B***, Corresponding quantification from three independent experiments. Error bars represent SEM. ***C–E***, Single-cell cultures from E8 dissociated chick retina were transfected with shRNAs against Atg7 to block autophagy, or with a control shRNA. ***C***, Analysis of retinal cultures after transfection of Atg7 shRNA and a plasmid for GFP-LC3 shows a downregulation of LC3-II puncta density compared with transfection with control shRNAs. ***D***, Reduction in axon branch density in axons transfected with Atg7 shRNA compared with controls. Axon length was not affected (***E***). ***C–E***, Error bars denote SEM. Statistical analyses were done using Student's *t* test; ***$p < 0.001$ and *$p < 0.05$; n.s., not significant.

mice with a full knock-out of Atg7, which showed a lack of formation of LC3-II (Komatsu et al., 2006).

In this series of experiments, we found that knock-down of Atg7 led to a reduction in overall axon branch density to 52.0 ± 6.52% (mean ± SEM; Fig. 6*D*) compared with cultures transfected with control shRNAs (100 ± 10.54%; mean ± SEM). This indicates that autophagy is affecting retinal axon branching.

Furthermore, we did not find statistically significant shifts in axon branch location between neurons transfected with Atg7 shRNA compared with control shRNA when investigating proximal and distal axonal thirds. In case of the proximal third, axon density in Atg7 shRNA expressing axons was reduced to 91.9 ± 13.3% (mean ± SEM) of control (100 ± 7.4%; $p = 0.608$ using Student's *t* test; $n = 11$), and was slightly increased to 103.8 ± 10.1% of control (100 ± 7.5%) for the distal third ($p = 0.752$ using Student's *t* test; $n = 10$). This suggests that global knock-down of Atg7 does not affect local axon branch location.

Axon length was not affected (Fig. 6*E*) suggesting that in particular the process of axon branching is sensitive to autophagy. Nevertheless, an increase in axon length after downregulation of autophagy has been observed for mouse primary cortical neurons (Ban et al., 2013), which ultimately suggests that autophagy affects different axon populations in different ways (Stavoe et al., 2016).

In a second, pharmacological approach (Fig. 7) to investigate the link between autophagy and axon branching, we used bafilomycin-A1, a drug that prevents lysosome acidification and abolishes autophagic flow (Klionsky et al., 2012). Retinal cultures were incubated with 10 nM bafilomycin-A1 for the last 24 h of the 3-d-long *in vitro* culture experiments (see Materials and Methods). This treatment strongly reduced the number of axon branches per unit length (Fig. 7*A*), with a branch density of 41.8 ± 5.7% (mean ± SEM), compared with 100 ± 0.7% (mean ± SEM) branches for dimethylsulfoxide (DMSO)-treated RGC axons. In this case axon length was reduced (Fig. 7*B*), suggesting that bafilomycin might have an effect also on other biological processes.

In parallel experiments, we analyzed whether bafilomycin at the concentration tested here leads to an abolishment/reduction in autophagy in retinal cultures (Gomez-Sintes et al., 2017). For this, we analyzed again the expression level of LC3-II (Klionsky et al., 2012); however, this time using Western blot analyses (Fig. 7*C*,*D*). We found a good correlation between the concentrations of bafilomycin-A1 in the retinal cultures and the level of LC3-II, meaning that retinal cultures at these developmental stages in fact show basal levels of autophagy (Boya et al., 2016) and that bafilomycin-A1 abolishes autophagic flow, i.e., a prevention of acidification of lysosomes prevents their fusion with autophagosomes and thus abolishes LC3-II degradation.

Induction of autophagy increases RGC axon branching

In the complementary approach, we investigated whether increasing autophagy leads to an increase in axon branch density (Fig. 7*E–G*). We used an approach that is based on findings showing that an activated mTORC1 pathway blocks autophagy. Treatment of retinal cultures with rapamycin, which inactivates the mTOR pathway, should therefore relieve this block, leading in turn to an increase in autophagy. To verify this, we transfected retinal cultures with LC3-mCherry, and analyzed the density of LC3-II-positive puncta in RGC axons after treatment with rapamycin (Fig. 7*E*; see Materials and Methods). We found that overnight treatment with 20 nM rapamycin significantly increased LC3-II puncta density in RGC axons (Fig. 7*E*), indicating that rapamycin indeed increases autophagy in these cells.

Using the same experimental paradigm, we then analyzed axon branch density. Our results show that treatment with 20 nM rapamycin overnight led to a statistically significant increase in axon branch density, compared with controls treated with DMSO only (Fig. 7*F*). Axon length was not affected (Fig. 7*G*).

Thus, our data are consistent with the idea that upregulation and downregulation of autophagy lead to an upregulation and downregulation of RGC axon branch density, respectively.

Arl8B controls axon branching through autophagy

To further scrutinize the link between Arl8B, axon branching and autophagy, we overexpressed Arl8B, but then asked whether the associated increase in axon branching (Fig. 2) could be eliminated by abolishing autophagy via knock-down

of Atg7, which decreases axon branches (Fig. 6). If this decrease were not observed, it would suggest that Arl8B controls axon branching using a pathway independent of autophagy.

However, our data show in fact that the Arl8-induced increase in branch density can be abolished by a knockdown of Atg7 (Fig. 7*H*) and is therefore in line with our principal hypothesis that Arl8B controls axon branching via lysosome/autophagosome positioning. Additionally, overexpression of Arl8B in the presence of rapamycin did not lead to a statistically significant increase in axon branching compared with overexpression of Arl8B alone (Fig. 7*H*).

Restricted colocalization of pre-SV clusters with Arl8B-positive vesicles, autophagosomes, and lysosomes

In view of the synaptotropic hypothesis which proposes a link between axon branching and presynapse formation (see Introduction), we then analyzed (1) whether pre-SV clusters colocalize with Arl8B, and (2) whether alterations in Arl8B expression level also shift the axonal position of pre-synapses, similar to the effects shown for lysosomes (Fig. 4) and autophagosomes (Fig. 5).

To label pre-SV s, we used an expression plasmid for synaptophysin tagged with GFP, syn-GFP. A confocal analysis of RGC axons 2 d after transfection of small amounts of respective expression plasmids showed a small colocalization between Arl8B-tdT puncta and syn-GFP puncta (Fig. 8*A–C*). A quantification by intensity correlation analysis using the ImageJ plugin 'coloc' (see Materials and Methods) demonstrates that this colocalization shows a statistically significant correlation (Pearson's correlation, $r = 0.45$; see Materials and Methods).

Although we observed only a limited synaptophysin/Arl8B colocalization, we investigated whether pre-SV distribution would change in response to an increase or decrease in the expression of Arl8B, aimed to uncover a (possible) link between positioning of pre-SV clusters and axon branches. We found that a downregulation of Arl8B using shRNA did not alter the relative SV2-puncta distribution along RGC axons compared with controls (Fig. 8*D*,*E*); however, a small decrease in the density of synaptophysin-positive puncta in the proximal third of axons was observed after Arl8B overexpression (Fig. 8*D*), suggesting rather an anti-correlation between positioning of pre-SV clusters and axon branching.

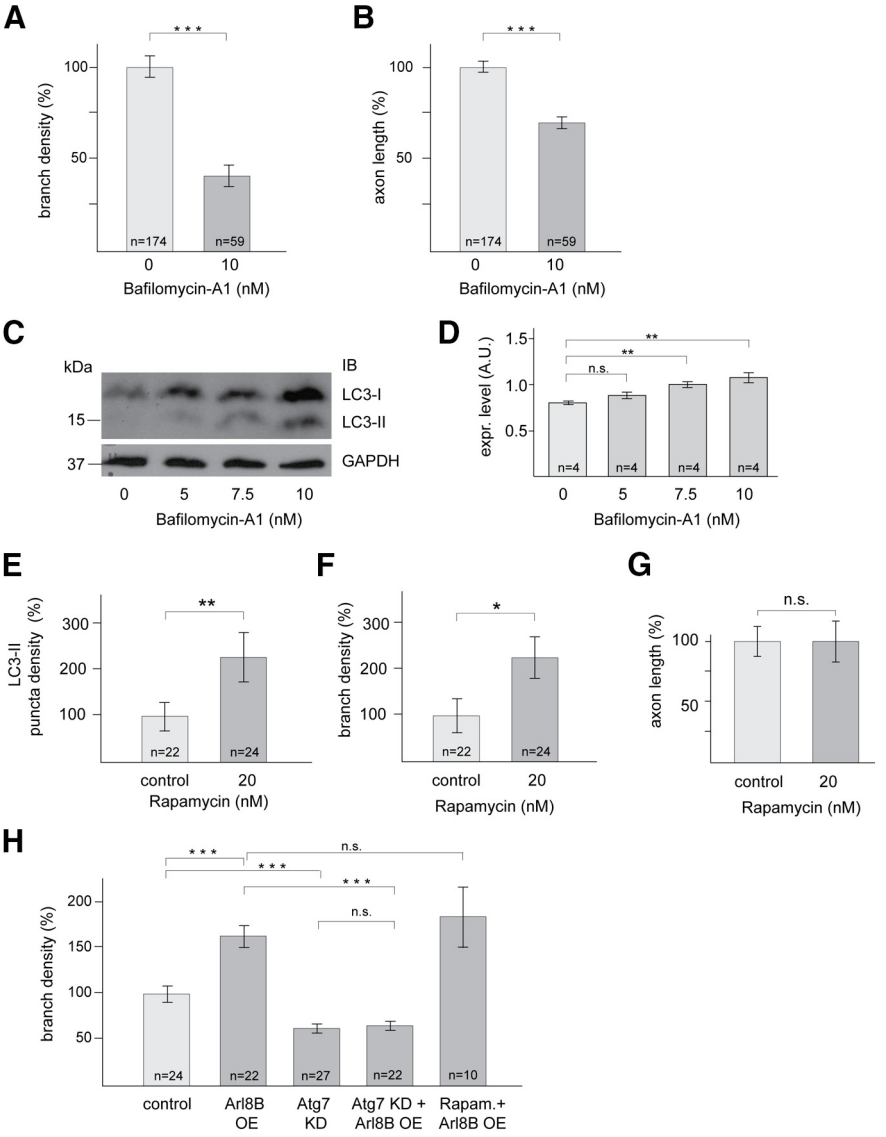

Figure 7. Pharmacological interference with autophagy affects axon branch density. ***A***, Axon branch density is reduced after incubation of retinal cultures with 10 nM bafilomycin-A1 for the last 24 h of 3-d-long experiments. ***B***, Under the same conditions, axon length is downregulated. ***C***, Western blot analysis of the expression levels of LC3-II, as an indicator for the block of autophagic flow triggered by bafilomycin-A1. GAPDH expression levels were determined as loading control. The Western blot image shows a representative of four independent experiments. ***D***, Corresponding quantification of band intensity (LC3-II) relative to GAPDH band intensity derived from four independent experiments. ***E–G***, Treatment of retinal cultures with 20 nM rapamycin results in an increase in LC3-II puncta density (***E***), and a >2-fold increase in axon branch density (***F***). Thus, the increase in autophagosome density indicates an increase in autophagy induction via a rapamycin-induced block of the mTOR pathway which normally inhibits autophagy (for details, see text). Axon length was not affected (***G***). ***H***, Arl8B exerts its effect on axon branching via autophagy-related pathways. Arl8B overexpression (OE) on its own results in an increase in branch density, while knock-down (KD) of Atg7 (abolishing autophagy) on its own leads to a decrease in branching. When combined, the Arl8-induced increase in branch density is abolished by the Atg7 known-down, suggesting that Arl8B exerts its effect on axon branching via an autophagy-related pathway. Overexpression of Arl8B in the presence of rapamycin to activate autophagosome formation results in a statistically insignificant increase in branch density compared with Arl8B OE only. The sum of results of two independent experiments is shown. Error bars denote SEM. Statistical analyses were done using Student's *t* test; $^{***}p < 0.001$, $^{**}p < 0.01$, $^{*}p < 0.05$; n.s., not significant. Data summarize the results of four (***C***, ***D***), three (***A***, ***B***), or two (***E–G***, ***H***) independently conducted experiments. The total number of axons analyzed (*n*) is given within the bars.

We also investigated a (possible) colocalization of pre-SV clusters with lysosomes and autophagosomes (Fig. 9). To monitor this, we transfected LC3-GFP into retinal cultures (Fig. 9*A–F*), which were then treated with bafilomycin-A1 to increase the likelihood of detecting LC3-positive puncta.

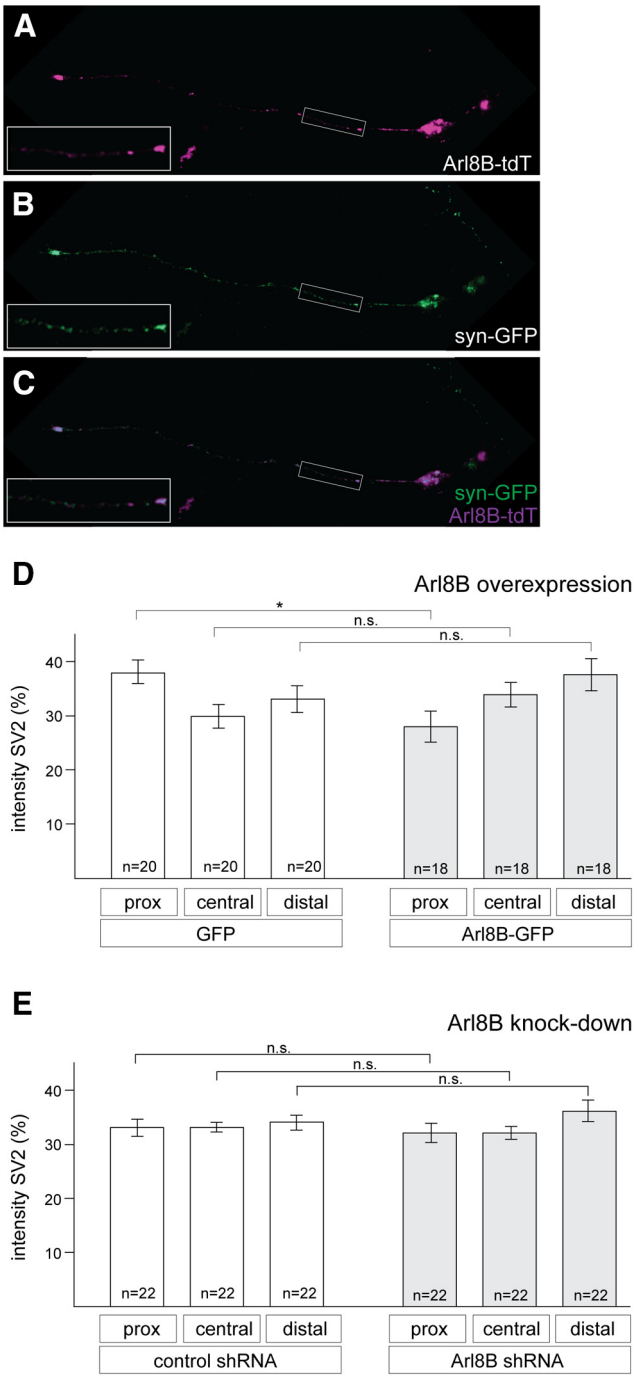

Figure 8. Limited colocalization between Arl8B and pre-SV clusters. ***A–C***, For a colocalization analysis, very small amounts of Arl8B-tdTomato and synaptophysin-GFP were transfected into single-cell retinal cultures, and investigated 3 d later. ***A***, Arl8B-tdTomato. ***B***, Synaptophysin-GFP. ***C***, Merger of ***A***, ***B***. See text for a quantitative description of the limited overlap between Arl8B and synaptophysin. ***D***, Distribution of synaptophysin-GFP-positive puncta along RGC axons after overexpression of Arl8B (using large amounts of Arl8B-GFP) or GFP (control). The pre-SV clusters were visualized by transfection of small amounts of synaptophysin-GFP. ***E***, Little changes in the distribution of synaptophysin-GFP-positive puncta along RGC axons after Arl8B knock-down, in comparison to control shRNA. Error bars denote SEM. Statistical analyses were done using Student's *t* test; $*p < 0.05$; n.s., not significant. Data summarize in each case the results of two independently conducted experiments. The total number of axons analyzed (*n*) is given within the bars.

For all axons analyzed, we found a weak though statistically significant correlation, indicating a (small) overlap between pre-SV clusters and LC3-II puncta (Pearson's correlation, $r = 0.46$; see Materials and Methods).

Similar data were obtained for a colocalization between SV2 and lysosomes with a Pearson's correlation of $r = 0.12$ (Fig. 9*G–L*).

In sum, these studies show a rather limited colocalization between pre-SV clusters on the one hand, and Arl8B, autophagosomes and lysosomes on the other hand. In fact, changing expression levels of Arl8B did not, or only little, affect pre-SV cluster positioning, which is in clear contrast with the obvious and consistent changes in autophagosome and lysosome positioning following Arl8B mis-expression. These results therefore suggest that Arl8B mediates its effect on axon branch density/positioning mainly through controlling (locally) autophagy-related processes but not through shifting pre-SV clusters.

Autophagy is necessary for proper formation of the retino-collicular projection

Next, we investigated whether interference with autophagy *in vivo* affects axon branching (Fig. 10), for which we used the mouse retino-collicular projection as a model, where RGC axons project from the eye to their main principle midbrain target, the superior colliculus (SC), in a topographic manner (for review, see Suetterlin et al., 2012; Cang and Feldheim, 2013). Based on our *in vitro* data (Fig. 6), the expectation was that blocking autophagy *in vivo* would lead to a reduction in RGC axon branching in the SC and thus a decrease in densities of the detected TZs.

For this approach, we used a mouse line in which the *atg7* gene, whose gene product is essential for autophagy and was targeted in our *in vitro* experiments (Fig. 6), can be conditionally inactivated using the cre/loxP system (Komatsu et al., 2006, 2007). These mice were crossed with a mouse line in which the Cre recombinase is expressed under control of the α-enhancer of the pax6 promoter whose activity is restricted to the nasal and temporal parts of the retina (α-*pax6:cre*; Marquardt et al., 2001). In homozygous $atg7^{fl/fl}$; cre^{+} offspring, autophagy is abolished only in these regions, leaving an unaffected area in the middle of the retina (Burbridge et al., 2014).

To confirm the expression of Cre in α-*pax6:cre* mice, we crossed these mice into a floxed- stop tdTomato reporter line (*Ai14*; https://www.jax.org/strain/007914) and verified the expression of tdTomato restricted to the temporal and nasal retina (Fig. 10*A*) and the projection pattern of (tdTomato-positive) temporal and nasal RGC axons to the rostral and caudal SC, respectively (Fig. 10*B*; Burbridge et al., 2014).

We then analyzed the offspring from crosses between heterozygous $atg7^{fl/+}$; cre^{+} mice ($atg7^{fl/+}$; cre^{+} x $atg7^{fl/+}$; cre^{+}). First, we investigated retina development in the offspring from these crosses (Fig. 10*C–F*), and found an apparently undisturbed, normal development of all retinal layers including the RGC layer in $atg7^{fl/fl}$; cre^{+} mice when compared with $atg7^{fl/fl}$; cre^{-} mice. A quantification of the fluorescence intensity of the DAPI stained RGC layer along the naso-temporal axis showed no apparent differences between nasal/temporal versus central regions, neither within or between $atg7^{fl/fl}$; cre^{+} and $atg7^{fl/fl}$; cre^{-} genotypes (Fig. 10*E–F*). This finding shows that the RGC layer contains similar numbers of cells suggesting that inactivation of autophagy does not affect normal development of RGCs at least up to P9.

Next, we investigated the projection pattern of nasal axons in the offspring from these crosses (Fig. 10*G–L*). For this, we injected a constant small amount of the lipophilic axon tracer DiI into the peripheral part of the nasal retina at postnatal day (P)8. The corresponding TZs in the SC were analyzed 1 d later at a developmental stage at which the retino-collicular projection is

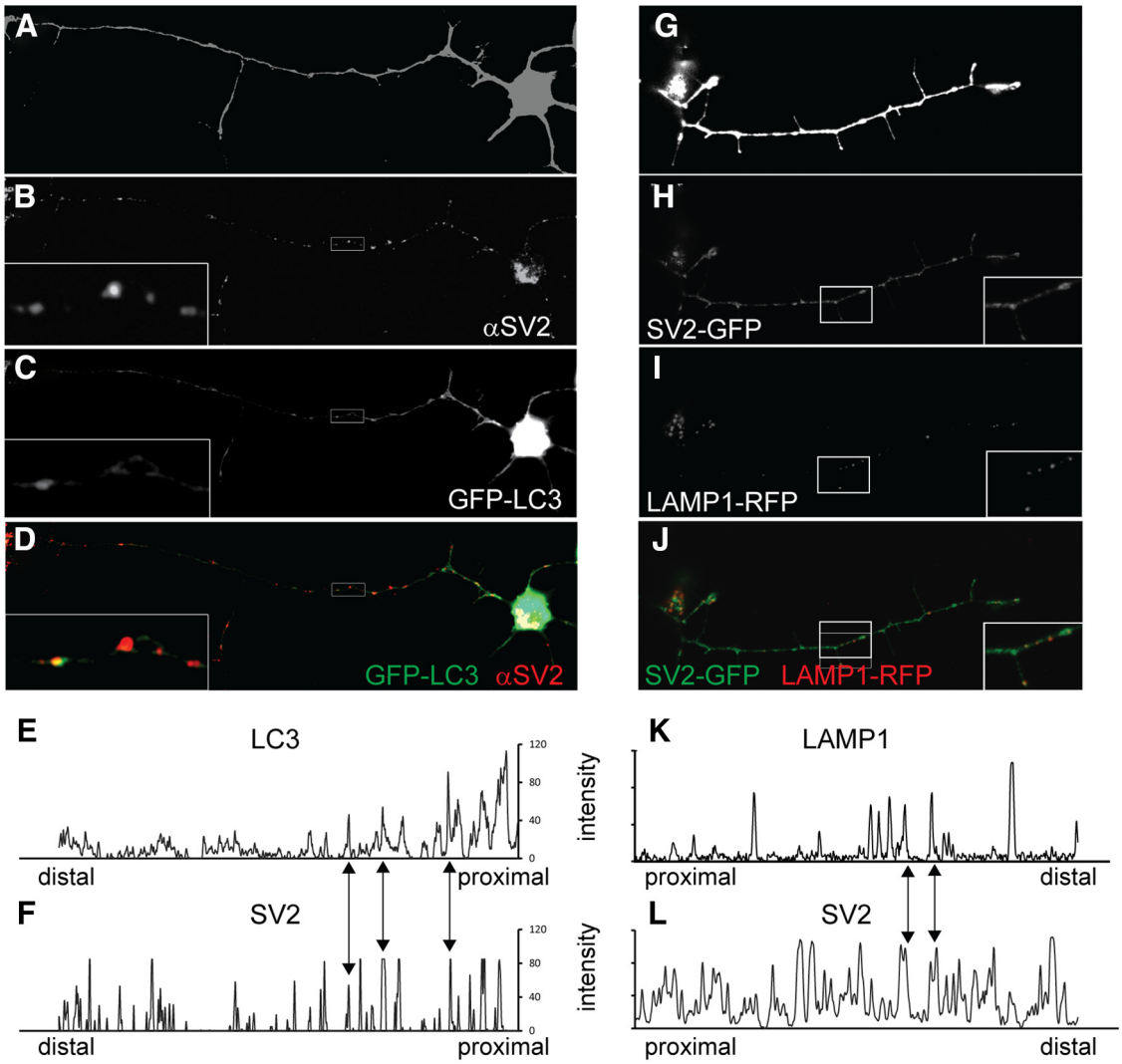

Figure 9. Limited colocalization of autophagosomes and lysosomes with pre-SV clusters on RGC axons. ***A–F***, Cultures prepared from E8 chick retina were transfected with small amounts of plasmids for GFP-LC3 expression to visualize LC3-II puncta (autophagosome) formation (***C***), incubated for 3 d and stained for SV2 to identify pre-SV clusters (***B***). ***A***, Morphology of the RGC of interest. ***D***, Merger of ***B***, ***C***. An area of partial colocalization between a pre-SV s cluster and a LC3-II punctum is shown enlarged in insets of ***B–D***. ImageJ 'coloc' programs show a small but significant overlap between SV2 and LC3-positive puncta (for details, see text and Materials and Methods). ***E***, ***F***, Graphical representations of pixel intensity of ***B***, ***C***. Areas of partial or full colocalization are indicated by vertical lines between ***E*** and ***F***. ***G–L***, Similar to experiments described in ***A–F***, retinal cultures were transfected with small amounts of synaptophysin-GFP (SV2-GFP; ***H***) and LAMP1-RFP (***I***), to analyze colocalizations between pre-SV clusters and lysosomes (***J***). ***G***, Scheme of the morphology of the RGC of interest. Insets in ***H***, ***J***, Area of partial colocalization between lysosomes and pre-SV clusters. ***K***, ***L***, Graphical representations of pixel intensity of ***H***, ***I***. Areas of partial or full colocalization are indicated by vertical lines between ***K*** and ***L***.

considered to be mature (Suetterlin and Drescher, 2014). Typical images from whole mounts (Fig. 10*G*,*H*) and parasagittal sections through the SC are shown (Fig. 10*I*,*J*). Using whole mount images, we then quantified the density of DiI-labeled TZs, defined as the sum of pixel intensities of the TZ divided by the area of the TZ (for details, see Materials and Methods) assuming that pixel intensity directly correlates with the amount of DiI-labeled axonal branches (Fig. 10*K*,*L*).

Our analysis showed that the TZ density in $atg7^{fl/fl}$; cre^{+} mice ($n = 17$) was significantly reduced to 53.7 ± 7.1% (mean ± SEM) when compared with controls [$atg7^{fl/fl}$; cre^{-}; $n = 11$; 100 ± 17.6% (mean ± SEM); $p < 0.05$; Fig. 10*G–J*]. The reduction in the density of the TZs suggests that inactivation of autophagy in the nasal retina results in a diminished connectivity of RGC axons in the SC, which correlates well with our results obtained in *in vitro* approaches (Fig. 6).

These two sets of data support the view that the reduction in TZ branch density in $atg7^{fl/fl}$; cre^{+} mice compared with $atg7^{fl/fl}$; cre^{-} mice is because of a disrupted connectivity pattern of RGC axons but not a defective retina development.

Discussion

Interstitial axon branching is a key step during the formation of neural circuits. Here, we have investigated the function of the GTPase Arl8B in this process, an adaptor molecule linking lysosomes to kinesin motor proteins. We show that up and down regulation of Arl8B leads to changes in the density and position of lysosomes and autophagosomes, and this together leads to changes in axon branch density and position. Direct abolition of autophagy reduces branch density, while increasing autophagy leads to an increase in branch density. *In vivo*, disruption of autophagy in the retina leads to a disturbance of the retino-collicular projection. Our data suggest that Arl8B controls the location of axon branches by controlling positioning of lysosomes and autophagosomes, that is by controlling local autophagy.

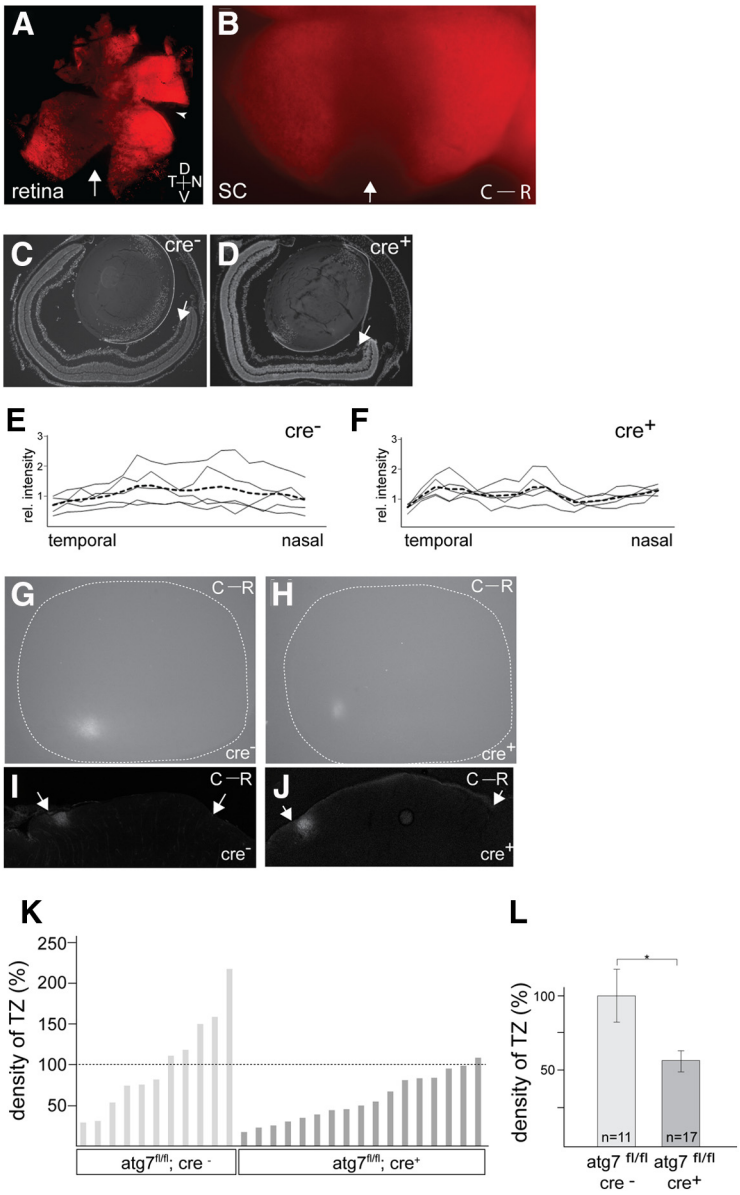

Figure 10. A retina-specific knock-out of autophagy disrupts retino-collicular map development. ***A***, ***B***, To demonstrate the restricted Cre expression in pax6-α:cre mice, the projection pattern of RGC axons was analyzed in a cross with Ai14 mice expressing tdTomato in a cre-dependent manner. ***A***, Flat-mounted retina at P7 showing a typical Cre-negative central dorso-ventral corridor (arrow) within an otherwise tdTomato-positive retina. The nasal cut (during preparation to orient the retina) is indicated by an arrowhead. Part of the temporal retina was omitted during preparation. ***B***, Dorsal view of a whole mount of a typical SC, showing a tdTomato-negative central corridor (arrow) along the dorso-lateral axis within an overall tdTomato-positive SC. The slight staining in the central corridor is because of axons crossing this area in the deeper SC layers eventually invading and forming TZs in the superficial part of the caudal/posterior SC. ***C–F***, DAPI staining of horizontal sections of representative retinae of *atg7*$^{fl/fl}$; *cre*$^{-}$ (***C***) and *atg7*$^{fl/fl}$; *cre*$^{+}$ (***D***) mice show undisturbed RGC layer formation in *atg7*$^{fl/fl}$; *cre*$^{+}$ mice. Arrows denotes the RGC layer. ***E***, ***F***, Quantification of fluorescence intensity of the RGC layer (as an indication of the number of cell nuclei; RGC layer labeled in ***C***, ***D***, with arrows) along the naso-temporal axis from five random different sections show no apparent differences between nasal/temporal versus central regions, neither within or between *atg7*$^{fl/fl}$; *cre*$^{+}$ and *atg7*$^{fl/fl}$; *cre*$^{-}$ genotypes. The dotted line indicates the average of all five densities. ***G–L***, Analysis of TZs of nasal RGC axons from either *atg7*$^{fl/fl}$; *cre*$^{+}$ or *atg7*$^{fl/fl}$; *cre*$^{-}$ mice. DiI was focally injected in the nasal periphery of P8 offspring from *atg7*$^{fl/+}$; *cre*$^{+}$ x *atg7*$^{fl/+}$; *cre*$^{+}$ crosses, and fluorescence microscopy of SC whole mounts (***G***, ***H***) was conducted 1 d later. Representative images from both genotypes of TZs in the posterior part of the SC are shown (same orientation as in ***B***). Overall, the TZs in *atg7*$^{fl/fl}$; *cre*$^{+}$ (***H***) appear weaker than in corresponding *atg7*$^{fl/fl}$; *cre*$^{-}$ controls (***G***). ***I***, ***J***, Parasagittal sections to further analyze TZs. Arrows indicate the rostral and caudal borders of the SC. Sections in ***I***, ***J*** are from different SCs than the whole mounts shown in ***G***, ***H***. Analysis was done blind to genotype. ***K***, ***L***, Quantification of TZ densities in *atg7*$^{fl/fl}$; *cre*$^{+}$ and *atg7*$^{fl/fl}$; *cre*$^{-}$ mice (see Materials and Methods). Densities of TZs in individual mice are shown in ***K***, and the sum for each genotype is shown in ***L***. The number of mice analyzed is given within the columns (***L***). The difference in densities between the two genotypes is statistically significant with $^{*}p < 0.05$. Error bars denote SEM. Statistical analyses were done using Student's *t* test; $^{*}p < 0.05$. Data summarize the results of two series of independently conducted injections. The total number of mice analyzed (*n*) is given within the bars. C: caudal; D: dorsal; N: nasal; R: rostral; T: temporal; V: ventral.

Correlation between Arl8B-mediated location of axon branches and lysosome positioning

Our principle finding that Arl8B, a GTPase specifically bound to lysosomes, is prominently involved in axon branch formation provides an entirely new avenue to understand the intracellular signaling controlling this process suggesting that in fact lysosomes are involved in this process.

Lysosomes exert multiple functions, and are not only involved in autophagy, but contribute to other processes including cell migration, formation of focal adhesions and membrane repair (for review, see Pu et al., 2016). Therefore, we characterized which of these canonical lysosome function/s are involved in controlling axon branching. For this, we demonstrate that also a direct interference with autophagy affects axon branching density, that is a decrease in autophagy reduces the density of RGC axon branches (Fig. 6), while an upregulation of autophagy increases branch density (Fig. 7). Furthermore, the Arl8B-mediated increase in branching could be abolished by knock-down of autophagy (Fig. 7*H*). This makes it likely that Arl8B in involved in axon branching by controlling autophagy-related lysosome functions.

Interestingly, autophagy is also required for dendritic branching (Clark et al., 2018); however, the mechanisms controlling dendritic branching must be different from those controlling axonal branching since Arl8B is not transported into dendrites (Farías et al., 2017).

An additional argument supporting our hypothesis is our finding that branching and autophagy are locally correlated, as visualized by the distribution of autophagosomes, which serve as a hallmark of autophagy. We found that upregulating Arl8B expression leads to an increase in lysosome and autophagosome density in the distal part of axons (Figs. 4, 5), and therefore in the same region as we detect an increase in axon branching. Similarly, downregulation of Arl8B leads to an increased density of lysosomes in the proximal part of axons (Fig. 4) in parallel to an increase in axon branches in the same region (Fig. 2).

Arl8B controls branching via autophagosome/lysosome interactions

How might an increased Arl8B expression lead to a higher density of autophagosomes in the distal axon? Normally, lysosomes preferentially form at the cell

body and are from here transported via Arl8B/kinesins/MTs into the axon, while autophagosomes form preferentially in the distal parts of the axon (Hollenbeck, 1993; Lee et al., 2011; Maday et al., 2012; Maday and Holzbaur, 2014; Cheng et al., 2015). Autophagosomes are retrogradely transported toward the cell body only *after* their fusion with lysosomes (autophagic flow; Maday et al., 2012). It is the fusion between lysosomes and autophagosomes which leads to an altered (activity) balance of motor proteins on these maturing autolysosomes which results in their retrograde transport back to the cell body.

After overexpression of Arl8B and in view of the function of Arl8B in relieving the kinesin autoinhibition, lysosomes appear to be linked to a much higher kinesin activity, i.e., a higher anterograde transport activity. Their fusion with autophagosomes would shift now the balance toward an anterograde transport, i.e., prevent a retrograde transport, and might therefore be the reason for the higher density of autophagosomes in the distal part of axons (Fig. 5), which is linked to a higher branch density.

Possible mechanism of axon branch induction by local autophagy

Based on the general concept that RGC axons are normally refractory to branching, we hypothesize that branching will occur only in regions where "suppressors" of axon branching have been removed by local (selective) autophagy (Fig. 11*A–C*). Thus, branching proceeds at locations devoid of suppressors (Fig. 11*D*). These locations will be determined by a set of factors produced by tectal cells, such as branch-promoting BDNF/TrkB and branch-suppressing EphA/ephrinA activities (Marler et al., 2008; Fig. 11).

Since debundling of MTs is a defining and early feature of interstitial branching (Kalil and Dent, 2014; Ketschek et al., 2015), prime intracellular targets of these combined TrkB/EphA signaling cascades could be molecules which normally suppress the debundling of MTs, such as MAP1B. In support of this view it has been shown that removal of MAP1B results in an increase of axon branching (Ketschek et al., 2015; Barnat et al., 2016). Moreover, the phosphorylated form of MAP1B preferentially interacts with autophagosomes (Wang et al., 2006; Yue, 2007), leading to a model in which the activation of upstream signaling cascades leads to the modification of the suppressor MAP1B. This now becomes now a target of autophagy and is removed, which allows axon branches to form and stabilize (Fig. 11).

Colocalization between Arl8B and pre-SV clusters

We found a small, but significant, colocalization between Arl8B-positive puncta (i.e., lysosomes and autophagosomes) and pre-SV clusters. However, we did not observe a change in the distribution of these presynapse clusters after overexpression or downregulation of Arl8B (Fig. 8) in a manner suggesting a correlation with axon branching. This lack of correlation therefore does not support a model in which presynapse formation and autophagy are entangled to control early steps of axon branching.

On the contrary, in a restricted number of neuronal populations in *C. elegans*, axonal autophagy and synapse development are functionally linked (Stavoe et al., 2016). Here, mutants in genes in the autophagy pathway lead to defects in synapse formation. However, this correlation was not found for most other neuronal classes in *C. elegans* (Stavoe et al., 2016) and seems therefore not to be a general principle of synapse formation.

Nevertheless, we cannot exclude that branch formation of RGC axons occurs from a sub-population of pre-SV clusters; however, these would be difficult to detect under our experimental conditions.

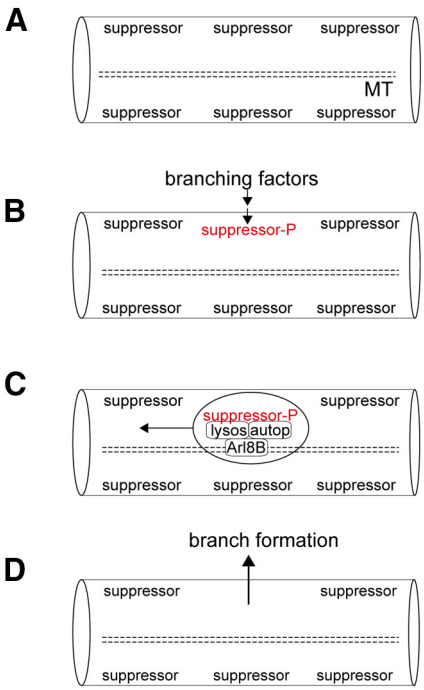

Figure 11. A model for axon branch induction by local autophagy. ***A***, An axon in its basic state is refractory to branch formation because of the presence of a hypothesized branch-suppressing activity (suppressor). ***B***, Locally acting branching factor/s modify this suppressor/s (-P). For RGC axons, good candidates are BDNF/TrkB as branch promoting and EphA/ephrinAs as branch-suppressing activities, which have been shown to interact (Marler et al., 2008), and whose balance might be crucial for the local formation of branches. ***C***, The modified suppressor/s are targeted by autophagosomes, which subsequently fuse with lysosomes, mediated by Arl8B. ***D***, The local removal of branch suppressors allows the local formation of branches.

Basal levels of autophagy are necessary for retino-collicular map formation

Little is known so far about the role of autophagy-related genes in establishing neural connectivity during development *in vivo*. However, the key autophagy kinases ULK1 and ULK2 do play a role in the development of the forebrain since respective knock-out mutants of these genes show defects in axonal pathfinding and de-fasciculation of major axonal tracts including the corpus callosum and the cortico-thalamic tract (Wang et al., 2018). Defects in formation of the major forebrain commissures were also observed for mutations in alfy (WDFY3), a scaffolding protein which facilitates the sorting of ubiquitinated cargo into autophagosomes (Dragich et al., 2016; Napoli et al., 2018).

We show here now, in good agreement with our *in vitro* data, that a retina-specific knock-out of autophagy leads to a disturbance of the formation of the retino-collicular projection. Nasal RGC axons from $atg7^{fl/fl}$; cre^{+} mice showed a significant reduction in the density of their TZs in the SC, compared with $atg7^{fl/fl}$; cre^{-} controls (Fig. 11). The restricted expression of Cre in the retina but not in the SC in *pax6-α:cre* mice (Fig. 11; Marquardt et al., 2001) allows the conclusion that these connectivity defects are specifically because of a block of autophagy in RGC axons and not because of alterations in the SC.

Outlook

Our *in vitro* and *in vivo* data presented here suggest that Arl8B controls the density and positioning of axon branches by regulating the transport of vesicles mediating locally autophagy. Future work will focus on the identification of factors with in turn

control the activity of Arl8B (Donaldson and Jackson, 2011; Niwa et al., 2017), the corresponding upstream signaling pathways (Marler et al., 2008), and the molecular mechanisms by which autophagy controls neural circuit formation *in vivo*.

References

Alsina B, Vu T, Cohen-Cory S (2001) Visualizing synapse formation in arborizing optic axons in vivo: dynamics and modulation by BDNF. Nat Neurosci 4:1093–1101.

Bagshaw RD, Callahan JW, Mahuran DJ (2006) The Arf-family protein, Arl8b, is involved in the spatial distribution of lysosomes. Biochem Biophys Res Commun 344:1186–1191.

Ban BK, Jun MH, Ryu HH, Jang DJ, Ahmad ST, Lee JA (2013) Autophagy negatively regulates early axon growth in cortical neurons. Mol Cell Biol 33:3907–3919.

Barnat M, Benassy MN, Vincensini L, Soares S, Fassier C, Propst F, Andrieux A, von Boxberg Y, Nothias F (2016) The GSK3-MAP1B pathway controls neurite branching and microtubule dynamics. Mol Cell Neurosci 72:9–21.

Bento CF, Puri C, Moreau K, Rubinsztein DC (2013) The role of membrane-trafficking small GTPases in the regulation of autophagy. J Cell Sci 126:1059–1069.

Boda A, Lörincz P, Takáts S, Csizmadia T, Tóth S, Kovács AL, Juhász G (2019) *Drosophila* Arl8 is a general positive regulator of lysosomal fusion events. Biochim Biophys Acta Mol Cell Res 1866:533–544.

Bonanomi D, Valenza F, Chivatakarn O, Sternfeld MJ, Driscoll SP, Aslanian A, Lettieri K, Gullo M, Badaloni A, Lewcock JW, Hunter T, Pfaff SL (2019) p190RhoGAP filters competing signals to resolve axon guidance conflicts. Neuron 102:602–620.e9.

Bonifacino JS, Neefjes J (2017) Moving and positioning the endolysosomal system. Curr Opin Cell Biol 47:1–8.

Boya P, Esteban-Martínez L, Serrano-Puebla A, Gómez-Sintes R, Villarejo-Zori B (2016) Autophagy in the eye: development, degeneration, and aging. Prog Retin Eye Res 55:206–245.

Burbridge TJ, Xu HP, Ackman JB, Ge X, Zhang Y, Ye MJ, Zhou ZJ, Xu J, Contractor A, Crair MC (2014) Visual circuit development requires patterned activity mediated by retinal acetylcholine receptors. Neuron 84:1049–1064.

Cang J, Feldheim DA (2013) Developmental mechanisms of topographic map formation and alignment. Annu Rev Neurosci 36:51–77.

Cheng XT, Zhou B, Lin MY, Cai Q, Sheng ZH (2015) Axonal autophagosomes recruit dynein for retrograde transport through fusion with late endosomes. J Cell Biol 209:377–386.

Chia PH, Chen B, Li P, Rosen MK, Shen K (2014) Local F-actin network links synapse formation and axon branching. Cell 156:208–220.

Cioni JM, Wong HH, Bressan D, Kodama L, Harris WA, Holt CE (2018) Axon-axon interactions regulate topographic optic tract sorting via CYFIP2-dependent WAVE complex function. Neuron 97:1078–1093.e6.

Cioni JM, Lin JQ, Holtermann AV, Koppers M, Jakobs MAH, Azizi A, Turner-Bridger B, Shigeoka T, Franze K, Harris WA, Holt CE (2019) Late endosomes act as mRNA translation platforms and sustain mitochondria in axons. Cell 176:56–72.e15.

Clark SG, Graybeal LL, Bhattacharjee S, Thomas C, Bhattacharya S, Cox DN (2018) Basal autophagy is required for promoting dendritic terminal branching in *Drosophila* sensory neurons. PLoS One 13:e0206743.

Cline H, Haas K (2008) The regulation of dendritic arbor development and plasticity by glutamatergic synaptic input: a review of the synaptotrophic hypothesis. J Physiol 586:1509–1517.

Constance WD, Mukherjee A, Fisher YE, Pop S, Blanc E, Toyama Y, Williams DW (2018) Neurexin and Neuroligin-based adhesion complexes drive axonal arborisation growth independent of synaptic activity. Elife 7:e31659.

Courchet J, Lewis TL Jr, Lee S, Courchet V, Liou DY, Aizawa S, Polleux F (2013) Terminal axon branching is regulated by the LKB1-NUAK1 kinase pathway via presynaptic mitochondrial capture. Cell 153:1510–1525.

Donaldson JG, Jackson CL (2011) ARF family G proteins and their regulators: roles in membrane transport, development and disease. Nat Rev Mol Cell Biol 12:362–375.

Dragich JM, Kuwajima T, Hirose-Ikeda M, Yoon MS, Eenjes E, Bosco JR, Fox LM, Lystad AH, Oo TF, Yarygina O, Mita T, Waguri S, Ichimura Y, Komatsu M, Simonsen A, Burke RE, Mason CA, Yamamoto A (2016) Autophagy linked FYVE (Alfy/WDFY3) is required for establishing neuronal connectivity in the mammalian brain. Elife 5:e14810.

Farías GG, Guardia CM, De Pace R, Britt DJ, Bonifacino JS (2017) BORC/kinesin-1 ensemble drives polarized transport of lysosomes into the axon. Proc Natl Acad Sci USA 114:E2955–E2964.

Feng Y, Yao Z, Klionsky DJ (2015) How to control self-digestion: transcriptional, post-transcriptional, and post-translational regulation of autophagy. Trends Cell Biol 25:354–363.

Ferguson SM (2018) Axonal transport and maturation of lysosomes. Curr Opin Neurobiol 51:45–51.

Filipek PA, de Araujo MEG, Vogel GF, De Smet CH, Eberharter D, Rebsamen M, Rudashevskaya EL, Kremser L, Yordanov T, Tschaikner P, Fürnrohr BG, Lechner S, Dunzendorfer-Matt T, Scheffzek K, Bennett KL, Superti-Furga G, Lindner HH, Stasyk T, Huber LA (2017) LAMTOR/Ragulator is a negative regulator of Arl8b- and BORC-dependent late endosomal positioning. J Cell Biol 216:4199–4215.

Furukawa N, Sakurai F, Katayama K, Seki N, Kawabata K, Mizuguchi H (2011) Optimization of a microRNA expression vector for function analysis of microRNA. J Control Release 150:94–101.

Gallo G (2011) The cytoskeletal and signaling mechanisms of axon collateral branching. Dev Neurobiol 71:201–220.

Galluzzi L, Pietrocola F, Levine B, Kroemer G (2014) Metabolic control of autophagy. Cell 159:1263–1276.

Garg S, Sharma M, Ung C, Tuli A, Barral DC, Hava DL, Veerapen N, Besra GS, Hacohen N, Brenner MB (2011) Lysosomal trafficking, antigen presentation, and microbial killing are controlled by the Arf-like GTPase Arl8b. Immunity 35:182–193.

Gillingham AK, Munro S (2007) The small G proteins of the Arf family and their regulators. Annu Rev Cell Dev Biol 23:579–611.

Goel P, Dufour Bergeron D, Bohme MA, Nunnelly L, Lehmann M, Buser C, Walter AM, Sigrist SJ, Dickman D (2019) Homeostatic scaling of active zone scaffolds maintains global synaptic strength. J Cell Biol 218:1706–1724.

Gomez-Sintes R, Villarejo-Zori B, Serrano-Puebla A, Esteban-Martinez L, Sierra-Filardi E, Ramirez-Pardo I, Rodriguez-Muela N, Boya P (2017) Standard assays for the study of autophagy in the ex vivo retina. Cells 6:37.

Harris H, Rubinsztein DC (2011) Control of autophagy as a therapy for neurodegenerative disease. Nat Rev Neurol 8:108–117.

Hindges R, McLaughlin T, Genoud N, Henkemeyer M, O'Leary DD (2002) EphB forward signaling controls directional branch extension and arborization required for dorsal-ventral retinotopic mapping. Neuron 35:475–487.

Hofmann I, Munro S (2006) An N-terminally acetylated Arf-like GTPase is localised to lysosomes and affects their motility. J Cell Sci 119:1494–1503.

Hollenbeck PJ (1993) Products of endocytosis and autophagy are retrieved from axons by regulated retrograde organelle transport. J Cell Biol 121:305–315.

Hurley JH, Schulman BA (2014) Atomistic autophagy: the structures of cellular self-digestion. Cell 157:300–311.

Jain A, Lamark T, Sjøttem E, Larsen KB, Awuh JA, Øvervatn A, McMahon M, Hayes JD, Johansen T (2010) p62/SQSTM1 is a target gene for transcription factor NRF2 and creates a positive feedback loop by inducing antioxidant response element-driven gene transcription. J Biol Chem 285:22576–22591.

Kalil K, Dent EW (2014) Branch management: mechanisms of axon branching in the developing vertebrate CNS. Nat Rev Neurosci 15:7–18.

Ketschek A, Jones S, Spillane M, Korobova F, Svitkina T, Gallo G (2015) Nerve growth factor promotes reorganization of the axonal microtubule array at sites of axon collateral branching. Dev Neurobiol 75:1441–1461.

Khatter D, Sindhwani A, Sharma M (2015a) Arf-like GTPase Arl8: moving from the periphery to the center of lysosomal biology. Cell Logist 5:e1086501.

Khatter D, Raina VB, Dwivedi D, Sindhwani A, Bahl S, Sharma M (2015b) The small GTPase Arl8b regulates assembly of the mammalian HOPS complex on lysosomes. J Cell Sci 128:1746–1761.

Klassen MP, Wu YE, Maeder CI, Nakae I, Cueva JG, Lehrman EK, Tada M, Gengyo-Ando K, Wang GJ, Goodman M, Mitani S, Kontani K, Katada T, Shen K (2010) An Arf-like small G protein, ARL-8, promotes the axonal transport of presynaptic cargoes by suppressing vesicle aggregation. Neuron 66:710–723.

Klionsky DJ, Abdalla FC, Abeliovich H, Abraham RT, Acevedo-Arozena A, Adeli K, Agholme L, Agnello M, Agostinis P, Aguirre-Ghiso JA, Ahn HJ, Ait-Mohamed O, Ait-Si-Ali S, Akematsu T, Akira S, Al-Younes HM, Al-Zeer MA, Albert ML, Albin RL, Alegre-Abarrategui J, et al. (2012) Guidelines for the use and interpretation of assays for monitoring autophagy. Autophagy 8:445–544.

Komatsu M, Waguri S, Chiba T, Murata S, Iwata J, Tanida I, Ueno T, Koike M, Uchiyama Y, Kominami E, Tanaka K (2006) Loss of autophagy in the central nervous system causes neurodegeneration in mice. Nature 441:880–884.

Komatsu M, Wang QJ, Holstein GR, Friedrich VL Jr, Iwata J, Kominami E, Chait BT, Tanaka K, Yue Z (2007) Essential role for autophagy protein Atg7 in the maintenance of axonal homeostasis and the prevention of axonal degeneration. Proc Natl Acad Sci USA 104:14489–14494.

Korolchuk VI, Saiki S, Lichtenberg M, Siddiqi FH, Roberts EA, Imarisio S, Jahreiss L, Sarkar S, Futter M, Menzies FM, O'Kane CJ, Deretic V, Rubinsztein DC (2011) Lysosomal positioning coordinates cellular nutrient responses. Nat Cell Biol 13:453–460.

Lee S, Sato Y, Nixon RA (2011) Lysosomal proteolysis inhibition selectively disrupts axonal transport of degradative organelles and causes an Alzheimer's-like axonal dystrophy. J Neurosci 31:7817–7830.

Lewis TL Jr, Kwon SK, Lee A, Shaw R, Polleux F (2018) MFF-dependent mitochondrial fission regulates presynaptic release and axon branching by limiting axonal mitochondria size. Nat Commun 9:5008.

Maday S, Holzbaur EL (2014) Autophagosome biogenesis in primary neurons follows an ordered and spatially regulated pathway. Dev Cell 30:71–85.

Maday S, Wallace KE, Holzbaur EL (2012) Autophagosomes initiate distally and mature during transport toward the cell soma in primary neurons. J Cell Biol 196:407–417.

Marler KJ, Becker-Barroso E, Martínez A, Llovera M, Wentzel C, Poopalasundaram S, Hindges R, Soriano E, Comella J, Drescher U (2008) A TrkB/EphrinA interaction controls retinal axon branching and synaptogenesis. J Neurosci 28:12700–12712.

Marler KJ, Suetterlin P, Dopplapudi A, Rubikaite A, Adnan J, Maiorano NA, Lowe AS, Thompson ID, Pathania M, Bordey A, Fulga T, Van Vactor DL, Hindges R, Drescher U (2014) BDNF promotes axon branching of retinal ganglion cells via miRNA-132 and p250GAP. J Neurosci 34:969–979.

Marquardt T, Ashery-Padan R, Andrejewski N, Scardigli R, Guillemot F, Gruss P (2001) Pax6 is required for the multipotent state of retinal progenitor cells. Cell 105:43–55.

Marwaha R, Arya SB, Jagga D, Kaur H, Tuli A, Sharma M (2017) The Rab7 effector PLEKHM1 binds Arl8b to promote cargo traffic to lysosomes. J Cell Biol 216:1051–1070.

Matsumoto N, Hoshiko M, Sugo N, Fukazawa Y, Yamamoto N (2016) Synapse-dependent and independent mechanisms of thalamocortical axon branching are regulated by neuronal activity. Dev Neurobiol 76:323–336.

McEwan DG, Popovic D, Gubas A, Terawaki S, Suzuki H, Stadel D, Coxon FP, Miranda de Stegmann D, Bhogaraju S, Maddi K, Kirchof A, Gatti E, Helfrich MH, Wakatsuki S, Behrends C, Pierre P, Dikic I (2015) PLEKHM1 regulates autophagosome-lysosome fusion through HOPS complex and LC3/GABARAP proteins. Mol Cell 57:39–54.

Meyer MP, Smith SJ (2006) Evidence from in vivo imaging that synaptogenesis guides the growth and branching of axonal arbors by two distinct mechanisms. J Neurosci 26:3604–3614.

Napoli E, Song G, Panoutsopoulos A, Riyadh MA, Kaushik G, Halmai J, Levenson R, Zarbalis KS, Giulivi C (2018) Beyond autophagy: a novel role for autism-linked Wdfy3 in brain mitophagy. Sci Rep 8:11348.

Niwa S, Lipton DM, Morikawa M, Zhao C, Hirokawa N, Lu H, Shen K (2016) Autoinhibition of a neuronal kinesin UNC-104/KIF1A regulates the size and density of synapses. Cell Rep 16:2129–2141.

Niwa S, Tao L, Lu SY, Liew GM, Feng W, Nachury MV, Shen K (2017) BORC regulates the axonal transport of synaptic vesicle precursors by activating ARL-8. Curr Biol 27:2569–2578.e4.

Ordonez DG, Lee MK, Feany MB (2018) α-Synuclein induces mitochondrial dysfunction through spectrin and the actin cytoskeleton. Neuron 97:108–124.e6.

Otsu N (1979) A threshold selection method from gray-level histograms. IEEE Trans Syst Man Cybern 9:62–66.

Pu J, Schindler C, Jia R, Jarnik M, Backlund P, Bonifacino JS (2015) BORC, a multisubunit complex that regulates lysosome positioning. Dev Cell 33:176–188.

Pu J, Guardia CM, Keren-Kaplan T, Bonifacino JS (2016) Mechanisms and functions of lysosome positioning. J Cell Sci 129:4329–4339.

Pu J, Keren-Kaplan T, Bonifacino JS (2017) A Ragulator-BORC interaction controls lysosome positioning in response to amino acid availability. J Cell Biol 216:4183–4197.

Rosa-Ferreira C, Munro S (2011) Arl8 and SKIP act together to link lysosomes to kinesin-1. Dev Cell 21:1171–1178.

Rosa-Ferreira C, Sweeney ST, Munro S (2018) The small G protein Arl8 contributes to lysosomal function and long-range axonal transport in *Drosophila*. Biol Open 7:bio035964.

Ruthazer ES, Li J, Cline HT (2006) Stabilization of axon branch dynamics by synaptic maturation. J Neurosci 26:3594–3603.

Shan Z, Lin Q, Deng C, Li X, Huang W, Tan H, Fu Y, Yang M, Yu XY (2009) An efficient method to enhance gene silencing by using precursor microRNA designed small hairpin RNAs. Mol Biol Rep 36:1483–1489.

Stavoe AK, Hill SE, Hall DH, Colón-Ramos DA (2016) KIF1A/UNC-104 Transports ATG-9 to Regulate Neurodevelopment and Autophagy at Synapses. Dev Cell 38:171–185.

Suetterlin P, Drescher U (2014) Target-independent ephrinA/EphA-mediated axon-axon repulsion as a novel element in retino-collicular mapping. Neuron 84:740– 713.

Suetterlin P, Marler KM, Drescher U (2012) Axonal ephrinA/EphA interactions, and the emergence of order in topographic projections. Semin Cell Dev Biol 23:1–6.

Tuli A, Thiery J, James AM, Michelet X, Sharma M, Garg S, Sanborn KB, Orange JS, Lieberman J, Brenner MB (2013) Arf-like GTPase Arl8b regulates lytic granule polarization and natural killer cell-mediated cytotoxicity. Mol Biol Cell 24:3721–3735.

Vaughn JE (1989) Fine structure of synaptogenesis in the vertebrate central nervous system. Synapse 3:255–285.

Vukoja A, Rey U, Petzoldt AG, Ott C, Vollweiter D, Quentin C, Puchkov D, Reynolds E, Lehmann M, Hohensee S, Rosa S, Lipowsky R, Sigrist SJ, Haucke V (2018) Presynaptic biogenesis requires axonal transport of lysosome-related vesicles. Neuron 99:1216–1232.e7.

Wang B, Iyengar R, Li-Harms X, Joo JH, Wright C, Lavado A, Horner L, Yang M, Guan JL, Frase S, Green DR, Cao X, Kundu M (2018) The autophagy-inducing kinases, ULK1 and ULK2, regulate axon guidance in the developing mouse forebrain via a noncanonical pathway. Autophagy 14:796–811.

Wang QJ, Ding Y, Kohtz DS, Kohtz S, Mizushima N, Cristea IM, Rout MP, Chait BT, Zhong Y, Heintz N, Yue Z (2006) Induction of autophagy in axonal dystrophy and degeneration. J Neurosci 26:8057–8068.

Weth F, Fiederling F, Gebhardt C, Bastmeyer M (2014) Chemoaffinity in topographic mapping revisited - Is it more about fiber-fiber than fiber-target interactions? Semin Cell Dev Biol 35:126–135.

Wong E, Cuervo AM (2010) Integration of clearance mechanisms: the proteasome and autophagy. Cold Spring Harb Perspect Biol 2:a006734.

Wong HH, Lin JQ, Ströhl F, Roque CG, Cioni JM, Cagnetta R, Turner-Bridger B, Laine RF, Harris WA, Kaminski CF, Holt CE (2017) RNA docking and local translation regulate site-specific axon remodeling in vivo. Neuron 95:852–868.e8.

Wu YE, Huo L, Maeder CI, Feng W, Shen K (2013) The balance between capture and dissociation of presynaptic proteins controls the spatial distribution of synapses. Neuron 78:994–1011.

Yates PA, Roskies AL, McLaughlin T, O'Leary DD (2001) Topographic-specific axon branching controlled by ephrin-as is the critical event in retinotectal map development. J Neurosci 21:8548–8563.

Yue Z (2007) Regulation of neuronal autophagy in axon: implication of autophagy in axonal function and dysfunction/degeneration. Autophagy 3:139–141.